

Nonequilibrium Josephson effect in mesoscopic ballistic multiterminal SNS junctions

P. Samuelsson, J. Lantz, V. S. Shumeiko, and G. Wendin

Department of Microelectronics and Nanoscience, Chalmers University of Technology and Göteborg University, S-41296 Göteborg, Sweden

(Received 20 April 1999; revised manuscript received 1 October 1999)

We present a detailed study of the nonequilibrium Josephson effect in quantum three- and four-terminal SNS devices. We focus our discussion on the anomalous dc Josephson current which is a prominent feature of open nonequilibrium quantum SNS structures. This current is revealed under tunnel injection and it grows with the applied voltage across the injection point, in sharp contrast to the effect of nonequilibrium population of the Andreev states which induces oscillations and sign reversal of the Josephson current as a function of injection voltage. The anomalous current does not decay with the length of the junction even in the long junction limit $L \gg \xi_T$. This long-range effect is microscopically connected to the similar property of the injection current. We study the resonant features in the dependence of the Josephson current and the injection current on the injection voltage and superconducting phase difference, discuss the effect of asymmetry (a crossover to π -periodic phase dependence) and the role of resistive NS interfaces which introduce additional, normal electron, resonances. The Josephson effect is qualitatively similar in three- and four-terminal junctions, while the injection current in four-terminal junctions exhibits a specific resonant behavior due to Fano resonances.

I. INTRODUCTION

The art of controlling Josephson current transport through mesoscopic superconducting junctions poses many challenges for theory and experiment from both fundamental and applied points of view. One possibility is to use a Josephson field effect transistor (JOFET),^{1,2} where control of the Josephson equilibrium current is imposed via an electrostatic gate. Another solution is to connect the normal region to a normal voltage biased reservoir. Injection of electrons and holes allows nonequilibrium quasiparticle distributions to be maintained in the N region, making it possible to control the *nonequilibrium* Josephson current. Recent progress in fabrication of superconducting junctions has brought forward a number of interesting multiterminal structures, e.g., two-dimensional electron gas, junctions,²⁻⁴ metallic junctions,^{5,6} and high- T_c junctions.⁷ The purpose of this paper is to provide a broad description of Josephson current transport through quantum SNS junctions under conditions of nonequilibrium in the normal region due to connection to a voltage biased normal reservoir.

The effect of nonequilibrium distribution of electrons in the normal region of SNS junctions was theoretically studied in the beginning of 1980s.⁸ These early studies were focused on nonstationary effects in long SNS junctions (effect of electromagnetic radiation, ac Josephson regime), where nonequilibrium leads to enhancement of the critical current at finite temperature. More recently, a similar problem was studied in classical and quantum superconducting point contacts where the nonequilibrium dc Josephson current can be suppressed and even reversed.⁹ The effect of the suppression and the reversal of the Josephson current under tunnel injection in multiterminal SNS junctions was first studied by van Wees, Lenssen, and Harmans¹⁰ in ballistic junctions and by Volkov¹¹ in diffusive junctions (see also Ref. 12). Suppression of the Josephson current due to injection has been experimentally demonstrated in both ballistic⁴ and diffusive

SNS junctions.⁵ Very recently, Baselmans *et al.*⁶ were able to experimentally reverse the direction of the Josephson current.

In ballistic junctions, the problem of nonequilibrium current injection is of particular interest: Andreev quantization in ballistic junctions¹³ provides means for achieving a dramatic variation of the nonequilibrium Josephson current. It has been found by Wendin and Shumeiko¹⁴ that nonequilibrium filling of Andreev levels may considerably *enhance* the critical current even at zero temperature as well as reverse the direction of the current. Various aspects of the nonequilibrium Josephson effect in ballistic junctions has been further analyzed in Refs. 15 and 16.

A further step beyond the work in Ref. 10 was taken by Samuelsson, Shumeiko, and Wendin¹⁶, who showed that modification of the Josephson current in ballistic junctions under injection does not reduce to the effect of nonequilibrium population. An essential aspect is the ability of the scatterer at the injection point to shift the phases of the quasiparticles. In such a case, the connection to the injection lead also affects the form of the wave function of the Andreev resonances, and therefore affects Josephson currents flowing through the resonances.

This is particularly dramatic for long junctions, where the equilibrium Josephson current is exponentially small at finite temperature.^{17,18} In contrast, the *anomalous* nonequilibrium Josephson current does not depend on the length of the junction (long-range Josephson effect).¹⁶ This means that, in principle, a dissipationless current of the order of the equilibrium Josephson current of a short junction can be restored under conditions of filling up all the Andreev levels in the gap. The effect is most pronounced in junctions with a small number of transport modes. This opens up the possibility for a new kind of Josephson transistor where the supercurrent is turned on when the gate voltage is switched from $eV=0$ to $eV=\Delta$.

The long-range Josephson effect associated with anomalous Josephson current¹⁶ must be distinguished from the so-

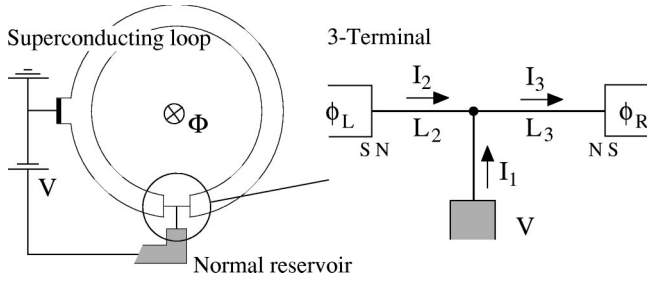


FIG. 1. A schematic picture of the three-terminal SNS junction setup under consideration, with a normal reservoir attached to the normal part of the junction. The normal reservoir is connected to the superconducting loop (grounded) via a voltage source biased at V . The right figure shows a closeup of the junction area with the arrows showing the direction of the current flow in the junction.

called dissipative Josephson effect.¹⁹ The latter consists of a net current flow between the superconducting electrodes as a result of asymmetric phase dependent splitting of the injection current. This current may flow in absence of a potential difference between the superconducting electrodes, in addition to the true Josephson current. In practice, these two effects may coexist and therefore the analysis of the injection current is a necessary element of the analysis of the nonequilibrium Josephson effect.

In this paper, we analyze the nonequilibrium Josephson effect in three- and four-terminal ballistic SNS junctions with different lengths and geometry, with transparent and resistive SN interfaces and for various temperatures.

The paper is organized as follows. In Sec. II, we present a general discussion of the currents in a 3-terminal SNS device. In Sec. III we describe our model based on the stationary Bogoliubov–de Gennes (BdG) equation. The derivation of all currents in the case of a three-terminal junction with transparent NS interfaces is presented in Sec. IV. In Sec. V, we discuss the equilibrium and nonequilibrium Josephson currents, both in a short and long junction; the effect of barriers at the NS interfaces is discussed in Sec. VI. The injection current and the normal conductance are analyzed in Sec. VII. In Sec. VIII we discuss four-terminal junctions.

II. NONEQUILIBRIUM JOSEPHSON CURRENTS

In this paper, we will consider two junction configurations: three and four terminal. The 3-terminal configuration (see Fig. 1) is an elementary structure which gives all necessary information for understanding the Josephson effect also in the four-terminal junction, to be discussed below. The normal part of the junction is inserted between two superconducting electrodes. The superconducting electrodes are connected with each other to form a loop and the magnetic flux threading the loop allows us to control the phase difference $\phi = \phi_R - \phi_L$ across the junction.

We consider a junction in the ballistic limit, when the length $L = L_2 + L_3$ of the normal part of the junction is shorter than both the elastic and inelastic scattering lengths, $L \ll l_e, l_i$. We use a simplified description of the connection point, modeling it by a scattering matrix S that connects incoming and outgoing wave-function amplitudes:²⁰

$$\Psi_{out} = S \Psi_{in}, \quad (1)$$

with

$$S = \begin{pmatrix} \sqrt{1-2\epsilon} & \sqrt{\epsilon} & \sqrt{\epsilon} \\ \sqrt{\epsilon} & r & d \\ \sqrt{\epsilon} & d & r \end{pmatrix}, \quad (2)$$

where r and d are reflection and transmission amplitudes for scattering between lead 2 and lead 3 and $\sqrt{\epsilon}$ is the scattering amplitude from the injection lead 1 to lead 2 or 3. In a multichannel treatment, r, d and ϵ become matrices describing the scattering between the channels. In this paper we however choose to consider a single-mode structure.

In the junction presented in Fig. 1, the current I_1 injected into the junction from the normal reservoir splits at the connection point. At the NS interfaces, the normal current is converted into a supercurrent. The supercurrent flows around the loop and is drained at a point connected to the normal reservoir via a voltage source biased at voltage V . There are two major questions about the currents: (i) what is the current I_1 in injection electrode 1 as function of the applied voltage and superconducting phase difference, and (ii) how is the current distributed between the arms 2 and 3?

The first problem has been discussed earlier,^{21–23} and the picture is the following: due to Andreev quantization the problem is equivalent to a resonant transmission problem. For weak coupling to the normal reservoir, $\epsilon \ll 1$, the probability of an incoming electron to be reflected is large unless its energy coincides with an Andreev level. In such a case, the electron is back scattered as a hole which produces a current density peak. The current as a function of applied voltage between the normal reservoir and the junction (IVC) thus increases stepwise, typical for resonant transport, with position and height of the steps depending on the phase difference between the superconductors.

The second question about current distribution between the junction arms concerns a subtle problem of the coexistence of the injection current flowing through the superconductor and the nonequilibrium Josephson current. Generally, the injected current asymmetrically splits between the two SN interfaces and induces a net phase-dependent current circulating within the loop without producing voltage drop across the SNS junction.¹⁹ This current flows in addition to the true Josephson current which is affected by the injection-induced nonequilibrium. Since only the total current in the loop can be measured, there is no way to distinguish the nonequilibrium Josephson current from the circulating injection current. However, the nonequilibrium Josephson current can be naturally *defined* in the limit of small coupling between the SNS junction and the normal reservoir, $\epsilon \rightarrow 0$: the injection current becomes vanishingly small in this limit and may be neglected, while the true Josephson current tends to a finite value. Following this definition, we will focus on the limit $\epsilon \ll 1$ when discussing the Josephson current below.

The scattering states carrying the current can qualitatively be described as electrons or holes entering the SNS junction from the injection lead 1, being split at the connection point, scattered back and forth in the junction by Andreev reflections at the NS interfaces and normal reflections at the connection point, and then finally leaving the junction, having effectively transported current from one superconductor to

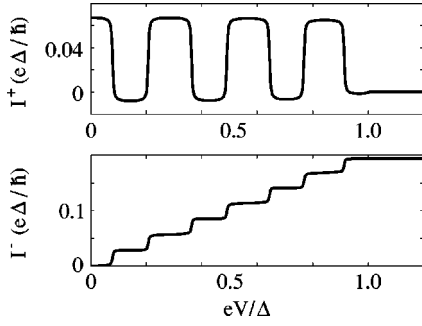


FIG. 2. The current voltage characteristics (IVC) for I^+ (upper) and I^- (lower) for a junction with seven Andreev levels for $0 < E < \Delta$. The currents jump every time the voltage eV is equal to the energy of an Andreev level, typical for resonant transport.

the other. When the dwell time \hbar/Γ at the Andreev resonances is smaller than the inelastic scattering time l_i/v_F in the junction, the quasiparticle distribution in the normal region is determined by the Fermi distribution function of the normal reservoir, and the current in the leads $j=2$ or 3 from injected quasiparticles can be written

$$I_j = \int_{-\infty}^{\infty} dE (i_j^e n^e + i_j^h n^h), \quad (3)$$

where $i_j^{e(h)}$ is the current density for injected electrons (holes) and $n^{e(h)} = n_F(E \pm eV)$ are the Fermi distribution functions in the normal reservoir, with $n_F = [1 + \exp(E/kT)]^{-1}$. The dwell time at the Andreev resonances is determined by the coupling to the reservoir ϵ and the spacing between resonances, roughly varying between Δ and $\hbar v_F/L$, depending on the length of the junction. This puts a lower constraint on the coupling constant ϵ , which thus has to obey the inequalities

$$L/l_i, \xi_0/l_i \ll \epsilon \ll 1, \quad (4)$$

where $\xi_0 = \hbar v_F/\Delta$.

The current in Eq. (3) can conveniently be rewritten

$$I_j = \int_{-\infty}^{\infty} dE \left[\frac{i_j^+}{2} (n^e + n^h) + \frac{i_j^-}{2} (n^e - n^h) \right] = I_j^+ + I_j^-, \quad (5)$$

where $i^+ = i^e + i^h$ and $i^- = i^e - i^h$. Quasiparticles are also injected from the superconductors for energies above the superconducting gap. Since the superconductors are grounded ($V=0$), the current from the superconductors is an equilibrium current. This current plus the current $I^+ = I_2^+ = I_3^+$ injected from the normal reservoir in absence of applied voltage, is the total equilibrium current. Applying a bias voltage ($V \neq 0$), I^+ becomes the nonequilibrium current due to population of the empty Andreev levels, giving rise to current jumps when the injection energy eV equals the Andreev level energies (see Fig. 2). This makes it possible to probe the energy of the Andreev levels.^{10,16,15}

The I^- part of the current is entirely nonequilibrium current. It partly consists of the injection current; however, there is also a component which does not vanish in the limit of weak coupling to the reservoir: we call this the anomalous Josephson current.¹⁶ This current results from a different form of the Andreev resonance wave functions in the open

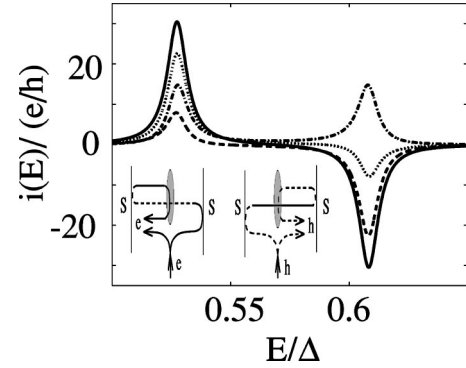


FIG. 3. The charge current density for two resonant Andreev levels for injected electrons i^e (dotted) and holes i^h (dashed), their sum i^+ (solid) and difference i^- (dash dotted). Note that the difference current i^- has the same sign for both resonances. Inset: Two lowest order paths for an injected electron (solid) or a hole (dashed) at a resonance. The gray ellipse denotes the effective scatterer due to the three lead connection. The difference of the currents due to these processes is proportional to $\text{Im}(rd^*)\sin\phi$, the first-order term of the anomalous current.

junction compared with the wave functions of true Andreev bound states. The origin of the anomalous current can qualitatively be described by considering the lowest order quasiparticle classical paths which contribute to the resonances in transparent junctions ($R \ll 1$) with perfect NS interfaces.

Consider a resonant state where the most of the electrons move to the left and the holes to the right, only a fraction of them traveling in the opposite direction due to normal scattering at the connection point. An injected electron gives rise to a left-going electron in lead 2 with the amplitude $1 + e^{i\phi_R} d^* e^{-i\phi_L} r$ with $\phi = \phi_R - \phi_L$ (not taking electron and hole dephasing and the energy dependent phase picked up when Andreev reflecting into account) thus giving a contribution to the current of the order $1 + RD + \text{Re}(rd^* e^{i\phi})$ (see inset in Fig. 3). Correspondingly, an injected hole gives rise to a right-going hole in lead 3 with amplitude $1 + e^{-i\phi_L} d e^{i\phi_R} r^*$ and a contribution to the current of order $1 + RD + \text{Re}(rd^* e^{-i\phi})$ (see right figure in inset in Fig. 3). The difference current i^- thus contains a part proportional to $\text{Re}[rd^*(e^{i\phi} - e^{-i\phi})] = 2\text{Im}(rd^*)\sin(\phi)$, which is the leading term in the anomalous current. At a resonant state where the particles move in the opposite direction, i.e., the electrons to the right and the holes to the left, we find from the same arguments that the anomalous current is again proportional to $2\text{Im}(rd^*)\sin(\phi)$, with the same sign. The anomalous current thus flows in the same direction for all resonances, in contrast to the equilibrium Josephson current which changes sign from one level to the next. The IVC for I^- is thus a staircase, as shown in Fig. 2, saturating at $eV > \Delta$ due to the absence of sharp resonances for energies above the superconducting gap. This has a dramatic effect on the long range properties of the Josephson current.

For a long junction ($L \gg \xi_0 = \hbar v_F/\Delta$), the IVC in Fig. 2 becomes dense, since there is a large number $\sim L/\xi_0$ of Andreev levels in the junction. The spacing between the Andreev levels is $\sim \hbar v_F/L$, so at temperatures exceeding the interlevel distance, the current I^+ is averaged to zero while I^- is reduced to a smooth ramp function. We thus get a current I^- that increases linearly with voltage up to $eV = \Delta$

and saturates at a level of the order of the equilibrium Josephson current of a short junction, $I \sim e\Delta/\hbar$. This current is independent of the length of the junction, since there is a large number of levels $\sim L$ each carrying a current $\sim 1/L$.

III. CALCULATION OF THE CURRENT

A. General formulation

We consider a three-terminal junction with asymmetric current injection ($L_2 \neq L_3$) and perfect transmission at the NS interfaces. The wave functions in the different regions of the junction are found from the stationary one-dimensional Bogoliubov–de Gennes equation²⁴

$$\begin{bmatrix} H_0 & \Delta \\ \Delta^* & -H_0 \end{bmatrix} \Psi = E\Psi, \quad H_0 = -\frac{\hbar^2}{2m} \frac{d^2}{dx^2} - E_F \quad (6)$$

which gives E as a departure from E_F . The wave functions are then matched at the NS interfaces and at the connection point, which gives the full scattering state wave function for injected quasiparticles. The cross section of the superconducting electrodes is much larger than the magnetic penetration depth, which allows one to control the phase difference by means of the magnetic flux Φ threading the superconducting loop (see Fig. 1). To neglect the effect of the magnetic field on the normal electrons in the SNS junction we assume that the area of the normal region of the junction is small compared to the area of the superconducting loop so that the magnetic flux through the normal region is much smaller than the flux quantum. In this case, a gauge in the normal region can be chosen such that the influence of magnetic field is fully accounted for by the superconducting phase difference, which in this case is gauge invariant. The electrostatic potential in the SNS junction is zero since the potential difference between the normal reservoir and the SNS junction drops at the injection point, due to rapid spreading out of the current in the normal reservoir.

Since the cross section of the normal region is assumed to be much smaller than the cross section of the superconducting electrodes (as indicated in Fig. 1), the influence of the normal region on the superconductors can be neglected. We apply the approximation²⁵ with $\Delta(x)$ constant in the superconductors and zero in the normal region,

$$\Delta(x) = \begin{cases} \Delta e^{i\phi_L} & x < -L_2 \\ 0 & -L_2 < x < L_3, \\ \Delta e^{i\phi_R} & x > L_3 \end{cases} \quad (7)$$

where the gauge invariant phase difference between the superconductors is $\phi = \phi_R - \phi_L$. We can then make an ansatz with plane waves in the different regions of the junction. For positive energies $E > 0$ we put in the normal regions $j = 1, 2, 3$,

$$\begin{aligned} \Psi_j = & c_j^{+,e} \begin{bmatrix} 1 \\ 0 \end{bmatrix} e^{ik^e x} + c_j^{h,-} \begin{bmatrix} 0 \\ 1 \end{bmatrix} e^{-ik^h x} \\ & + c_j^{e,-} \begin{bmatrix} 1 \\ 0 \end{bmatrix} e^{-ik^e x} + c_j^{h,+} \begin{bmatrix} 0 \\ 1 \end{bmatrix} e^{ik^h x} \end{aligned} \quad (8)$$

and in the superconductors $j = L, R$

$$\begin{aligned} \Psi_j = & d_j^{e,+} \begin{bmatrix} u e^{i\phi_j} \\ v \end{bmatrix} e^{iq^e x} + d_j^{h,-} \begin{bmatrix} v e^{i\phi_j} \\ u \end{bmatrix} e^{-iq^h x} \\ & + d_j^{e,-} \begin{bmatrix} u e^{i\phi_j} \\ v \end{bmatrix} e^{-iq^e x} + d_j^{h,+} \begin{bmatrix} v e^{i\phi_j} \\ u \end{bmatrix} e^{iq^e x}. \end{aligned} \quad (9)$$

The wave functions are normalized to unit amplitude of the incoming quasiparticles. The upper and lower components u and v of the wave function are defined as

$$u(+), v(-) = \begin{cases} \sqrt{\frac{1}{2}(1 \pm \xi/E)} & E > \Delta \\ \sqrt{\frac{1}{2}(E \pm \xi)/\Delta} & E < \Delta \end{cases}, \quad (10)$$

where $\xi = \sqrt{E^2 - \Delta^2}$ for $E > \Delta$ and $\xi = i\sqrt{\Delta^2 - E^2}$ for $E < \Delta$. The wave vectors are $q^{e,h} = \sqrt{2m/\hbar^2} \sqrt{E_F \pm \xi}$ in the superconductors and $k^{e,h} = \sqrt{2m/\hbar^2} \sqrt{E_F \pm E}$ in the normal regions. The wave functions are matched at the NS interfaces and at the injection point. The three-terminal injection point is modeled by the scattering matrix^{20,21} given by Eq. (2). The scattering amplitudes ϵ ($0 \leq \epsilon \leq 0.5$), d and r obey the relations $\text{Re}(rd^*) = -\epsilon/2$ and $D + R = 1 - \epsilon$ ($D = |d|^2, R = |r|^2$) due to the unitarity of the scattering matrix. Moreover, $\text{Im}(rd^*) = \sigma\sqrt{RD - \epsilon^2}/4$, with $\sigma = \pm 1$ dependent on the phase of the scatterer. For simplicity the coupling parameter ϵ is chosen real and positive. The scattering amplitudes are assumed to be energy independent, which gives the scattering matrix for hole wave-function amplitudes $S_h = S_e^*$.

Assuming $\Delta \ll E_F$ we make the approximation $q^e = q^h = k_F$ in the superconductors and $k^e = k^h = k_F$ in the normal region except in exponentials where we put $k^{e,h} = k_F \pm E/(\hbar v_F)$. At energies $E < \Delta$, only electrons and holes from the normal reservoirs are injected in the junction. For $E > \Delta$ quasiparticles from the superconductors are also injected. The current of the scattering states in the three normal regions are calculated following the Landauer–Büttiker scattering approach.²⁶ The spectral current density in region j is given by

$$i_j(E) = \frac{e}{h} (|c_j^{+,e}|^2 - |c_j^{-,e}|^2 + |c_j^{+,h}|^2 - |c_j^{-,h}|^2). \quad (11)$$

We now define energy dependent phases $\theta_{2,3} = \gamma - \beta_{2,3}$ in each of the leads 2 and 3, consisting of the phase $\gamma = \arccos(E/\Delta)$ picked up by the electrons and holes when Andreev reflecting, and the dephasing $\beta_{2,3} = (k^e - k^h)L_{2,3} = 2EL_{2,3}/(\hbar v_F)$ of the electrons and holes while propagating ballistically through the normal region. Furthermore, it is convenient to separate out the specific features of asymmetry by introducing sum phases $2\theta = \theta_2 + \theta_3$, $\beta = \beta_2 + \beta_3$, and the difference phases $\chi = \theta_2 - \theta_3$, defining essential phase parameters characterizing the junction,

$$\theta = \gamma - \beta/2 = \arccos(E/\Delta) - EL/(\hbar v_F), \quad (12)$$

$$\chi = \beta_3 - \beta_2 = 2El/(\hbar v_F), \quad (13)$$

where $L = L_2 + L_3$ and $l = L_3 - L_2$

The current densities of the scattering states in leads 2 and 3 from electrons $i_{2,3}^e$ and holes $i_{2,3}^h$ are then given by

$$i_2^{e,h} = -\frac{e}{h} \frac{\epsilon}{Z} (2D \sin \phi \sin 2\theta \pm \{\sigma 2 \sqrt{RD - \epsilon^2/4} \sin \phi (\cos \chi - \cos 2\theta) + \epsilon [1 - \cos(2\gamma - \beta_2) + \cos \phi (\cos \chi - \cos 2\theta)]\}), \quad (14)$$

$$i_3^{e,h} = -\frac{e}{h} \frac{\epsilon}{Z} (2D \sin \phi \sin 2\theta \pm \{2\sigma \sqrt{RD - \epsilon^2/4} \sin \phi (\cos \chi - \cos 2\theta) - \epsilon [1 - \cos(2\gamma - \beta_3) + \cos \phi (\cos \chi - \cos 2\theta)]\}) \quad (15)$$

with the superscript $e(h)$ related to $+$ ($-$) and where

$$Z = [(1 - \epsilon) \cos 2\theta - R \cos \chi - D \cos \phi]^2 + \epsilon^2 \sin^2 2\theta. \quad (16)$$

From Eqs. (14) and (15) it follows that the sum of the electron and hole current densities, $i^+ = i^e + i^h$, are equal in leads 2 and 3, giving the sum current density

$$i^+ = i_3^+ = i_2^+ = -\frac{4e}{h} \frac{\epsilon}{Z} \{D \sin \phi \sin 2\theta\}. \quad (17)$$

The difference current densities $i^- = i^e - i^h$ in leads 2 and 3 are not equal, however. We therefore define the anomalous current density i_a as that part of the difference current density which survives in the limit $\epsilon \rightarrow 0$,

$$i_a = -\sigma \frac{4e}{h} \frac{\epsilon}{Z} \{\sqrt{RD - \epsilon^2/4} \sin \phi (\cos \chi - \cos 2\theta)\}. \quad (18)$$

The injection current density $i_{inj} = i_3^- - i_2^-$ is given by,

$$i_{inj} = \frac{4e}{h} \frac{\epsilon^2}{Z} \{\sin^2 \chi + (\cos \chi + \cos \phi)(\cos \chi - \cos 2\theta)\} \quad (19)$$

and splits asymmetrically between the two horizontal arms 2 and 3,

$$i_{inj2,3} = \pm \frac{2e}{h} \frac{\epsilon^2}{Z} \{1 - \cos(2\theta - \beta_{2,3}) + \cos \phi (\cos \chi - \cos 2\theta)\}. \quad (20)$$

From the relations $i^+(E) = -i^+(-E)$ and $i^-(E) = i^-(-E)$ one can calculate the current densities for all energies inside the gap $|E| < \Delta$. The continuum current density, for energies outside the gap $|E| > \Delta$, is calculated in the same way. However, since the Andreev reflection probability decays very rapidly outside the gap, the Andreev resonances become very broad and contribute much less to the current. Only the quasiparticles injected from the superconductors contribute significantly to the current, as will be discussed below. The full formulas for the continuum current density for a symmetric junction $l=0$ is presented in Appendix A.

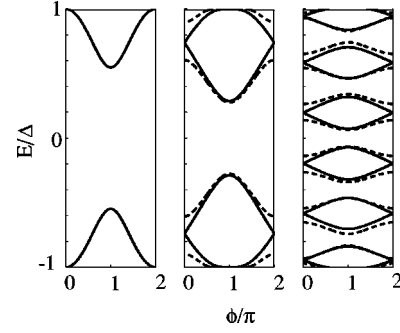


FIG. 4. Andreev bound state energies as a function of phase difference ϕ for different lengths $L=0$ (left), $L \sim \xi_0$ (middle), and $L \gg \xi_0$ (right) of the junction with $D=0.7$. Solid lines are for a symmetric junction $l=0$, dashed for an asymmetric one. A gap opens up in the spectrum at $\phi=0$ due to the asymmetry.

B. Weak-coupling limit

In the limit of small coupling to the reservoir, $\epsilon \ll 1$, the Andreev resonances are very sharp and the current densities are calculated by evaluating the expression ϵ/Z appearing in the Eqs. (17)–(19), in the limit $\epsilon \rightarrow 0$. This is done in detail in Appendix B, and gives [see Eq. (B6)]

$$\lim_{\epsilon \rightarrow 0} \frac{\epsilon}{Z} = \sum_{n,\pm} \frac{\pi}{D |\sin \phi \sin 2\theta|} \left| \frac{dE}{d\phi} \right| \delta(E - E_n^\pm). \quad (21)$$

where E_n^\pm are the energies of the bound Andreev states. To calculate the current density, information about the bound state energies as well as the derivative of the energy with respect to phase difference is thus needed. The bound state energies are given by the zeros of the denominator Z [Eq. (16)] at $\epsilon=0$, namely²⁷

$$\cos 2\theta = R \cos \chi + D \cos \phi. \quad (22)$$

The energy of the Andreev levels as a function of phase difference ϕ is plotted in Fig. 4. In the figure it is shown that the Andreev levels appear in pairs, labeled by n , with an upper ($+$) and a lower ($-$) level (referring to $E > 0$). The index n is zero for the pair of levels with positive energy closest to E_F . In the case of one single bound state, the level is labeled by E_0^- .

The derivative of the bound state energy with respect to phase is obtained by differentiating Eq. (22), giving

$$\frac{dE_n^\pm}{d\phi} = \frac{D \sin \phi}{2 \sin 2\theta} \left(\frac{1}{\sqrt{\Delta^2 - (E_n^\pm)^2}} + \frac{L}{\hbar v_F} + \frac{l}{\hbar v_F} R \frac{\sin \chi}{\sin 2\theta} \right)^{-1}. \quad (23)$$

The expression for the sum current density is given by inserting Eqs. (21)–(23) into Eq. (17), giving

$$i^+ = \frac{2e}{h} \sum_{n,\pm} \frac{dE}{d\phi} \delta(E - E_n^\pm), \quad (24)$$

where the relation $\text{sgn}[(dE/d\phi) \sin \phi \sin 2\theta] = -1$ [see Eq. (B9)] has been taken into account. The expression (24) coincides with the equation for the Andreev bound state current²⁸ derived directly from the BdG equation. From the alternating slopes of the energy-phase relation $E(\phi)$, plotted

in Fig. 4, it is clear that the sum current density ($\sim dE/d\phi$) changes sign between two subsequent Andreev resonances (see Fig. 3).

The anomalous current density i_a is given directly by inserting Eq. (21) into Eq. (18), namely

$$i_a = -\sigma \frac{2e}{\hbar} \text{sgn}(\sin \phi) \sqrt{RD} \times \sum_{n,\pm} \frac{\cos \chi - \cos \phi}{|\sin 2\theta|} \left| \frac{dE_n^\pm}{d\phi} \right| \delta(E - E_n^\pm). \quad (25)$$

For a symmetric junction $l=0, \cos \chi=1$, the anomalous current density does not change sign as a function of energy, opposite to the sum current density (see Fig. 3). For finite asymmetry, the anomalous current might change sign. However, this does not lead to strong suppression of the total anomalous current, as will be shown below in Sec. VB.

The injection current $i_{inj} = i_3^- - i_2^-$ goes to zero for $\epsilon \ll 1$. We approximate the injection current in the weak-coupling limit by the first-order term in ϵ , given by inserting the expression for ϵ/Z in the zero coupling limit into Eq. (21),

$$i_{inj} = \epsilon \frac{8e}{\hbar} \sum_{n,\pm} \frac{\sin^2 \chi + D(\cos \chi - \cos \phi)^2}{|\sin 2\theta|} \times \left| \frac{dE_n^\pm}{d\phi} \right| \delta(E - E_n^\pm). \quad (26)$$

The injection current density is closely related to the anomalous current density i_a , in the sense that the injection current density is positive for all energies and values of the phase difference ϕ .

C. Structure of the nonequilibrium current

Including the continuum contribution from the superconductors (Appendix A) in Eq. (5), we can finally write down the structure of the total current in each lead:

$$I_j = \int_{-\infty}^{\infty} dE \left[\frac{i_j^+}{2} (n^e + n^h) + \frac{i_j^-}{2} (n^e - n^h) + i^s n_F \right], \quad (27)$$

where i^s is the current density from the quasiparticles injected from the superconductors. The equilibrium current ($V=0$) flowing in leads 2 and 3 is given by

$$I_{eq} = \int dE [i^+ + i^s] n_F \quad (28)$$

while in lead 1 it is zero. Subtracting the equilibrium current from the total current we get the nonequilibrium current in the horizontal leads 2 and 3. We divide the nonequilibrium current into the regular current I_r associated with the non-equilibrium population of the existing resonant states,

$$I_r = \int dE \left[\frac{i^+}{2} (n^e + n^h - 2n_F) \right], \quad (29)$$

the anomalous current I_a associated with the essential modification of the Andreev states due to the open normal lead,

$$I_a = \int dE \left[\frac{i_a}{2} (n^e - n^h) \right], \quad (30)$$

and the injected current I_1 ,

$$I_1 = I_{inj} = \int dE \left[\frac{i_{inj}}{2} (n^e - n^h) \right]. \quad (31)$$

With these definitions, the total currents in leads 2 and 3 may be written as

$$I_2 = I_{eq} + I_r + I_a - I_{inj,2}, \quad (32)$$

$$I_3 = I_{eq} + I_r + I_a + I_{inj,3},$$

where $I_{inj} = I_{inj,2} + I_{inj,3}$. As discussed in Sec. II, the separation of the anomalous current is arbitrary, and has physical meaning only in the weak-coupling limit when $I_{inj} \rightarrow 0$.

In the weak-coupling limit, the integrals in Eqs. (29) and (30) become sums over resonant states,

$$I_r = \frac{e}{\hbar} \sum_{n,\pm} \frac{dE_n^\pm}{d\phi} [n^e(E_n^\pm) + n^h(E_n^\pm) - 2n_F(E_n^\pm)], \quad (33)$$

$$I_a = -\sigma \frac{e}{\hbar} \text{sgn}(\sin \phi) \sqrt{RD} \times \sum_{n,\pm} \frac{\cos \chi - \cos \phi}{|\sin 2\theta|} \left| \frac{dE_n^\pm}{d\phi} \right| [n^e(E_n^\pm) - n^h(E_n^\pm)]. \quad (34)$$

The equilibrium current for energies $|E| < \Delta$ is given by inserting Eq. (24) into Eq. (28),

$$I_{eq}^b = \frac{2e}{\hbar} \sum_{n,\pm} \frac{dE_n^\pm}{d\phi} n_F(E_n^\pm). \quad (35)$$

For energies above the gap, the equilibrium current results from quasiparticles injected from the superconductors only, since this current is the only continuum current being finite in the weak-coupling limit (see Appendix A).

IV. JOSEPHSON CURRENT OF A SHORT JUNCTION

For a short junction $L=l=0$, there is exactly one resonance for positive energies $0 < E < \Delta$. For no coupling to the normal reservoir $\epsilon=0$, this resonant Andreev state is converted into a bound Andreev state, with the dispersion relation $E_0^- = \Delta \sqrt{1 - D \sin^2(\phi/2)}$. The equilibrium current of a short junction is thus given by the well-known²⁹ relation

$$I_{eq} = \frac{e\Delta}{\hbar} \frac{D \sin \phi}{2\sqrt{1 - D \sin^2(\phi/2)}} \tanh(E_0^-/2kT). \quad (36)$$

The continuum current is zero, which can be seen by putting $L=0$ ($\beta=0$) in the equations for the continuum current in Appendix A. At zero temperature and zero applied bias, only the level with negative energy $-E_0^-$ is populated. For an applied voltage bias $V > 0$, the electron (hole) population is shifted upwards (downwards) in energy. When the voltage $eV = E_0^-$, the energy of the resonant level, the level becomes populated and there is an abrupt jump of the current. The

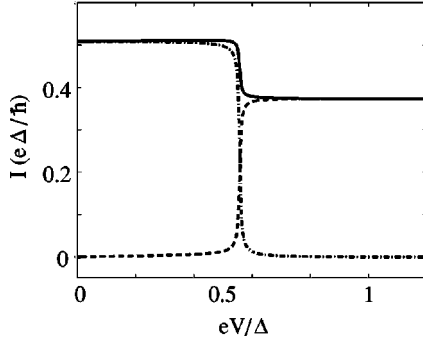


FIG. 5. The currents $I_{eq} + I_r$ (dash dotted), I_a (dashed), and the total Josephson current $I_{eq} + I_r + I_a$ (solid) in the horizontal leads 2 and 3 as a function of voltage V at $T=0$ for a short junction $L=0$ with $D=0.8$, $\phi=3\pi/4$, $\epsilon=0.01$, and $\sigma=-1$. The total current is I_{eq} for $eV < E_0^-$ and δI_a for $eV > E_0^-$.

regular part of the current, I_r , jumps an amount $\delta I_r = -I_{eq}$, thus cancelling the equilibrium Josephson current (see Fig. 5). This has recently been observed in experiments.^{4,5} The anomalous current jumps by the amount

$$\delta I_a = \sigma \frac{e\Delta}{2\hbar} \frac{\sqrt{RD} \sin \phi |\sin \phi/2|}{1 - D \sin^2(\phi/2)} \quad (37)$$

and is thus the total current of the junction. The effect of finite temperature in a zero length junction is merely to smear the steps in the IVC.

In the symmetric case ($l=0$) it is interesting to extend the discussion to a longer junction with two resonant levels (see Fig. 4), since the current distribution between the levels becomes nontrivial.^{14,15} In the limit $D \ll 1$, both resonances have energies close to the gap edge, $E_0^\pm \approx \Delta$, and with the additional approximation $\beta/2 > \sqrt{D}$ we obtain the expression for the derivative of energy with respect to phase [see Eq. (23)],

$$\frac{dE_0^\pm}{d\phi} = \pm \frac{\Delta \sqrt{D}}{4} \frac{L}{\xi_0} \frac{\sin(\phi)}{|\sin(\phi/2)| \sqrt{1 - D \sin^2(\phi/2)}}. \quad (38)$$

The equilibrium bound state current becomes proportional to $I_{eq}^b \sim dE_0^+/d\phi + dE_0^-/d\phi \sim D$ (taking terms of order D into account), but for the currents of the individual levels $\sim \sqrt{D}$. The resonant levels thus carry opposite ‘‘giant’’ currents which almost cancel in equilibrium. For $L > 0$, we also have to take the continuum contribution into account. It has been shown¹⁴ that the continuum contribution to the equilibrium current is $I_{eq}^c = -1/2 I_{eq}^b$, thus giving the total equilibrium current $I_{eq} = 1/2 I_{eq}^b$.

At zero temperature, when a voltage equal to the lowest lying level $eV = E_0^-$ is applied, the regular and anomalous current jumps,

$$\delta I_r = \frac{e\Delta}{\hbar} \frac{L}{\xi_0} \frac{\sqrt{D} \sin(\phi)}{2|\sin(\phi/2)| \sqrt{1 - D \sin^2(\phi/2)}}, \quad (39)$$

$$\delta I_a = \sigma \frac{e\Delta}{\hbar} \frac{L}{\xi_0} \frac{\sqrt{RD} \sin \phi}{\sqrt{1 - D \sin^2(\phi/2)}}. \quad (40)$$

Both jumps are proportional to \sqrt{D} , and the magnitude of the total current at $E_0^- < eV < E_0^+$ is then much larger than the equilibrium current.

When the bias voltage is further increased to $eV = E_0^+$ there is a second current jump: the regular current jumps in the *opposite* direction and becomes equal to the small negative bound state equilibrium current $I_r = -I_{eq}^b$. The anomalous current, however, again jumps δI_a in the *same* direction. For voltages $eV > E_0^+$ the total current in the junction is thus $I_{eq}^c + 2\delta I_a$. The full formulas for all the individual currents including temperature dependence is given in Appendix C.

V. JOSEPHSON CURRENT OF A LONG JUNCTION

We first discuss the Josephson current in a long ($L \gg \xi_0$) symmetric ($l=0$) junction. The junction length is limited by the requirement of Eq. (4), that the injected quasiparticles do not scatter inelastically in the junction, $L \ll \epsilon l_i$.

In a long junction there are many ($N = [L/(\xi_0 \pi)]$) pairs of resonances, as seen in Fig. 4. The derivative of energy with respect to phase $dE/d\phi$ in Eq. (23), which determines the current in Eqs. (33)–(35), can be simplified in a long junction $L \gg \xi_0$,

$$\frac{dE^\pm}{d\phi} = \pm \frac{\hbar v_F}{L} \frac{\sqrt{D} \sin(\phi)}{4|\sin(\phi/2)| \sqrt{1 - D \sin^2(\phi/2)}}. \quad (41)$$

This expression holds everywhere [with accuracy $O(1/L^3)$] except close to the gap edge, $\Delta - E_n \sim (\hbar v_F/L)(\xi_0/L)$, a distance much smaller than the energy distance $\pi \hbar v_F/L$ between the pairs of levels. Therefore Eq. (41) can be used for calculation of the currents of all levels except the last pair of levels closest to the energy gap.

A. Equilibrium current

The behavior of the equilibrium Josephson current, both at zero and finite temperature, is the result of fine compensation of the partial bound state and continuum state currents. According to Eqs. (41) and (23), each of the Andreev levels carries a current of order $1/L$, while each pair of levels carries a smaller net current of order $dE_n^+/d\phi - dE_n^-/d\phi \sim (1/L)^3$. Thus the equilibrium current of all bound states,

$$I_{eq}^b = \frac{e}{\hbar} \frac{\hbar v_F}{L} \frac{\sqrt{D} \sin(\phi)}{2|\sin(\phi/2)| \sqrt{1 - D \sin^2(\phi/2)}} \times \sum_{n=0}^{N-1} [\tanh(E_n^-/2kT) - \tanh(E_n^+/2kT)] + i^* \tanh(\Delta/2kT), \quad (42)$$

is determined at $T=0$ by the current from the last pair of levels at $E \approx \Delta$, $I_{eq}^b = i^* \sim 1/L$. This results in an oscillatory behavior of the bound state current with the junction length (see Fig. 6). A similar result was obtained for a fully transparent SNS junction in Ref. 30.

The continuum current in Eq. (A4) oscillates in the opposite sense, as also shown in Fig. 6, compensating the oscillations of the bound state current, Eq. (A5). As a result, the total current monotonously decays as $1/L$,^{31,32}

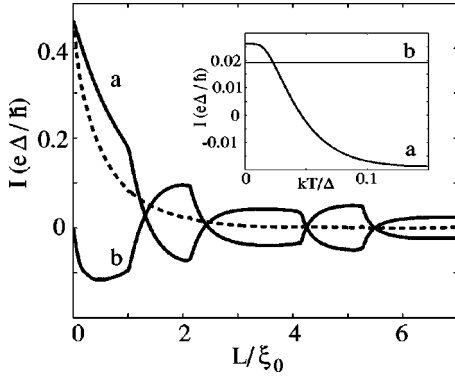


FIG. 6. The equilibrium bound state (a) and continuum (b) currents and their sum (dashed) as a function of length L for finite $kT=0.2\Delta$, $D=0.8$, $\phi=3\pi/4$, and $\epsilon=0.01$. There is a cusp in both the bound state and continuum currents when a new bound state forms out of the continuum. The total equilibrium current, however, dies monotonically with increased length. Inset: The equilibrium bound state and continuum currents as a function of temperature for a long junction $L=15\xi_0$ with $D=0.8$, $\phi=3\pi/4$, and $\epsilon=0.01$. The bound state current (a) decreases from $I_{eq}^b(T=0)=i^*$ to $-I_{eq}^c$, when the temperature is increased from zero to $kT \ll \hbar v_F/L$. The continuum current (b) is unaffected in this temperature regime.

$$I_{eq}(T=0) = \frac{e}{\hbar} \frac{\hbar v_F}{L} \frac{\sqrt{D} \sin(\phi) \arccos(R + D \cos \phi)}{2\pi |\sin(\phi/2)| \sqrt{1 - D \sin^2(\phi/2)}}. \quad (43)$$

When the temperature increases, the sum in Eq. (42) starts to contribute with negative sign, while the continuum current (and also i^*) is independent of temperature for $kT \ll \Delta$, since it is an integral over states with $|E| > \Delta$, Eq. (A4). The total current therefore rapidly decreases with temperature and becomes exponentially small for $kT \gg \hbar v_F/L$,^{17,32}

$$I_{eq}(kT \gg \hbar v_F/L) = \frac{e}{\hbar} 8kTD \sin \phi e^{-2\pi L/\xi_T}, \quad (44)$$

where $\xi_T = \hbar v_F/kT$.

B. Regular current

The regular current can be written, inserting relation (41) into Eq. (33), on the form

$$I_r = \frac{e}{\hbar} \frac{\hbar v_F}{2L} \frac{\sqrt{D} \sin(\phi)}{2|\sin(\phi/2)| \sqrt{1 - D \sin^2(\phi/2)}} \times \sum_{n=0}^{N-1} [g(E_n^-) - g(E_n^+)] + \frac{i^*}{2} g(\Delta), \quad (45)$$

where $g(E) = \tanh[(E+eV)/2kT] + \tanh[(E-eV)/2kT] - 2 \tanh(E/2kT)$. The regular current I_r jumps up or down every time $eV = E_n^\pm$ [see Fig. 7]. Each current jump has the magnitude

$$\delta I_r = \frac{e}{\hbar} \frac{\hbar v_F}{L} \frac{\sqrt{D} \sin(\phi)}{2|\sin(\phi/2)| \sqrt{1 - D \sin^2(\phi/2)}} \quad (46)$$

at zero temperature. At voltages $eV > \Delta$, the regular current is the sum of all states in the range $0 < E < \Delta$, and is equal to

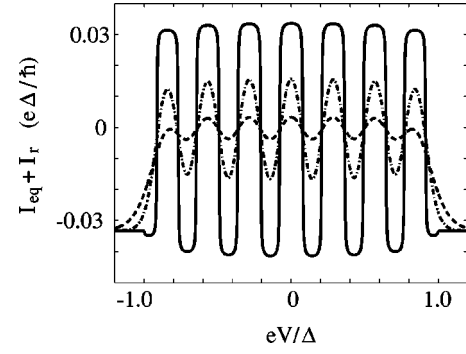


FIG. 7. The equilibrium current I_{eq} plus the regular current I_r vs voltage. $L=10\xi_0$, $\phi=\pi/2$, $D=0.8$, $\epsilon=0.05$. Solid line: $T=0$, dashed dotted: $kT=0.04\Delta$, dashed: $kT=0.07\Delta$. The regular current jumps alternating by $\pm \delta I_r$ every time the voltage is equal to the energy of an Andreev resonance. For $kT \gg \hbar v_F/L$ and $eV > \Delta$ the current $I_{eq} + I_r = I_{eq}^c$.

the negative bound state current $-i^*$, as is clear from the discussion in the previous section (Sec. V A).

It is interesting to study the sum $I_{eq} + I_r$, plotted in Fig. 7, at temperatures $kT \gg \hbar v_F/L$. In this temperature regime the equilibrium current is exponentially small and also the regular current steps in the IVC in Fig. 7 are suppressed. For a voltage $eV \sim \Delta$, the last level, carrying the major part (i^*) of the bound state current, is populated and the current $I_{eq} + I_r$ jumps to I_{eq}^c , the value of the continuum current, since all bound states are populated. This current I_{eq}^c is of the order of $1/L$ and the current $I_r + I_{eq}$ increases at $eV \sim \Delta$ from zero to a finite value $\sim 1/L$.

C. Anomalous current

The anomalous current is given by inserting Eq. (41) into Eq. (34),

$$I_a = -\sigma \frac{e}{\hbar} \frac{\hbar v_F}{4L} \frac{\sqrt{RD} \sin \phi}{1 - D \sin^2(\phi)} \sum_{n=0}^{N-1} [h(E_n^+) + h(E_n^-)], \quad (47)$$

where $h(E) = \tanh[(E-eV)/2kT] - \tanh[(E+eV)/2kT]$. We have neglected the current from the last level close to $E = \Delta$, because the currents of all levels add up and the current from the last level is negligible. The IVC at zero temperature looks like a staircase, as shown in Fig. 8.

The magnitude of the current step at zero temperature is given by

$$\delta I_a = \frac{e}{\hbar} \frac{\hbar v_F}{2L} \frac{\sqrt{RD} \sin \phi}{1 - D \sin^2(\phi/2)}. \quad (48)$$

At temperatures larger than the interlevel distance, $kT \gg \hbar v_F/L$, the staircase IVC is smeared out to a straight slope, as shown in Fig. 8. The exact position of each level becomes irrelevant and we can write the sum over bound states in Eq. (47) as an integral, noting that the expression $dE/dn = \pi \hbar v_F/L$ holds for all levels in the sum (47),

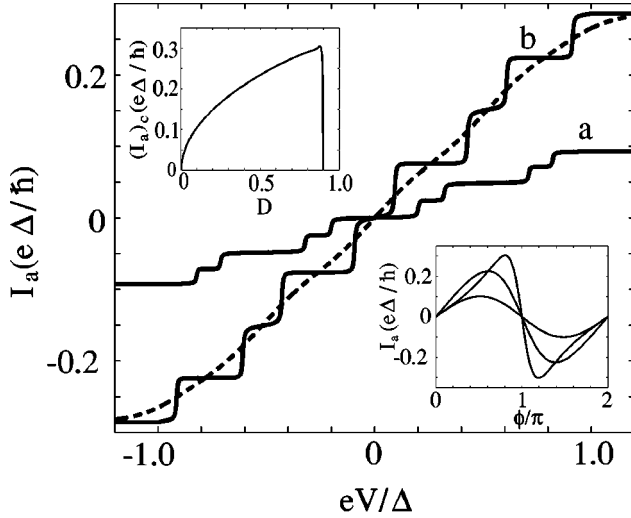


FIG. 8. The anomalous current as a function of voltage V for (a) $\phi = \pi/4$ and (b) $\phi = 3\pi/4$ for $L = 10\xi_0$, $D = 0.8$, $\epsilon = 0.05$, and $\sigma = -1$. Temperature $T = 0$ (solid) and $T = 0.1\Delta$ (dashed line). The current steps with magnitude δI_a are smeared to a straight line for $kT \gg \hbar v_F/L$. Upper inset: The critical anomalous current at $eV = \Delta$ as a function of transparency D for coupling constant $\epsilon = 0.1$. Due to finite coupling ϵ , the critical current always goes to zero for $R = 0$. Lower inset: The anomalous current $I_a(eV = \Delta, kT \gg \hbar v_F/L)$ as a function of phase difference ϕ for different transparencies $D = 0.1, 0.5$, and 0.9 . The highest amplitude corresponds to the highest transparency and vice versa.

$$\begin{aligned} & \sum_{n=0}^N [h(E_n^+) + h(E_n^-)] \\ & \approx \frac{2L}{\pi \hbar v_F} \int_0^\Delta dE [\tanh(E + eV) - \tanh(E - eV)] \\ & = \frac{4L}{\hbar v_F \pi} f(V, T), \end{aligned} \quad (49)$$

where

$$f(V, T) = kT \ln \left(\frac{\cosh(\Delta + eV)/kT}{\cosh(\Delta - eV)/kT} \right), \quad (50)$$

and the anomalous current takes the simple form

$$I_a = -\sigma \frac{e}{\hbar} \frac{\sqrt{RD} \sin \phi}{\pi [1 - D \sin^2(\phi/2)]} f(V, T). \quad (51)$$

In the limit $\hbar v_F/L \ll kT \ll \Delta$, $f(V, T) = \min(eV, \Delta)$: the anomalous current thus scales linearly with applied voltage up to Δ . It follows from Eq. (51) that I_a is independent of the length of the junction, being the sum of $N \sim L$ levels which each carries a current $I_n \sim 1/L$. This gives that the anomalous current roughly is equal to the total equilibrium current of the short junction. The critical anomalous current is plotted with respect to transparency in the inset in Fig. 8. In the limit $D \ll 1$ it is given by $(I_a)_c = (e/\hbar)(\sqrt{D}/\pi)f(V, T)$. It is proportional to the first power of Δ for T close to T_c , therefore surviving up to $kT \approx \Delta$. The anomalous current-phase relation (see inset in Fig. 8) is 2π periodic and resembles that of the equilibrium Josephson current. The direction of the

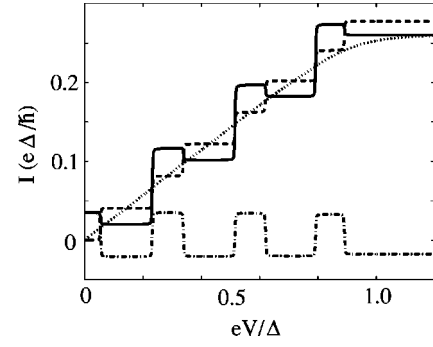


FIG. 9. The total current $I = I_{eq} + I_r + I_a$ as a function of voltage. At zero temperature we have $I_r + I_{eq}$ (dash dotted), I_a (dashed), and the total current $I_r + I_{eq} + I_a$ (solid). The total current for temperatures $kT \gg \hbar v_F/L$ is plotted (dotted). Junction parameters are $D = 0.8$, $\phi = 3\pi/4$, $L = 20\xi_0$, $\epsilon = 0.01$, and $\sigma = -1$.

anomalous current is however proportional to σ , i.e., dependent on the phase of the scatterer at the connection point, which is not the case for the equilibrium Josephson current.

To get the complete picture of the Josephson current in a long junction, $I = I_{eq} + I_r + I_a$ is plotted as a function of bias voltage for different temperatures in Fig. 9.

The zero-temperature total Josephson current oscillates strongly around a constant slope as a function of voltage, showing steps whenever the voltage passes an Andreev level. The step structures are washed out for temperatures $kT \gg \hbar v_F/L$, and in this limit the total current roughly coincides with the anomalous current, given by Eq. (51).

D. Asymmetric junction

The effect of asymmetry is most pronounced in the long limit when the asymmetry is much larger than the coherence length but much smaller than the total length of the junction, $L \gg l \gg \xi_0$. In this limit, the derivative of energy with respect to phase $dE/d\phi$ in Eq. (23) reduces to the expression of a symmetric long junction (41), since $|\sin 2\theta| > R|\sin \chi|$ (see Appendix B). The equilibrium current I_{eq} and the regular current I_r are not substantially changed in comparison to the symmetric case. In contrast, the anomalous current is modified in a nontrivial way, taking the form

$$\begin{aligned} I_a & = -\sigma \frac{e}{\hbar} \frac{\hbar v_F}{L} \sqrt{RD}^{3/2} \sin \phi \\ & \times \sum_{n,\pm}^N \frac{\cos \chi - \cos \phi}{1 - (D \cos \phi + R \cos \chi)^2} (n^e - n^h), \end{aligned} \quad (52)$$

obtained by inserting Eq. (41) into Eq. (34). For $T = 0$ the step structure in the IVC is modified due to the change of Andreev levels as a result of the asymmetry (see Fig. 4). Already for small asymmetry $l \sim \xi_0$ the anomalous current might change dramatically (see Fig. 10). Depending on the phase difference of the junction, the IVC is renormalized and changes sign for $-\pi/2 < \phi < \pi/2$.

When the temperature is increased beyond the interlevel distance $kT \gg \hbar v_F/L$, the step structure becomes smeared and we get a periodic modulation of the IVC on the scale of $eV \sim \hbar v_F/l$. This modulation arises from the factor $\cos \chi$.

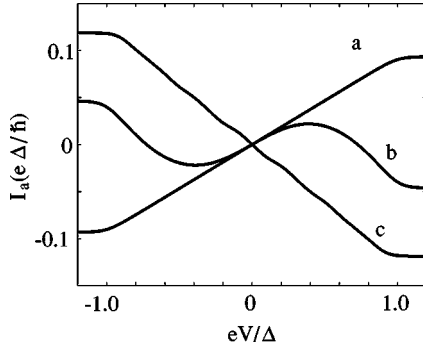


FIG. 10. The asymmetric anomalous current I_a vs voltage for different asymmetries (a) $l=0\xi_0$, (b) $l=2\xi_0$, and (c) $l=40\xi_0$ for $kT \gg \hbar v_F/L$, $D=0.8$, $\epsilon=0.05$, $L=60\xi_0$, $\phi=\pi/4$, and $\sigma=-1$. The IVC is changed dramatically already for as small asymmetry $l \sim \xi_0$, if the phase difference $-\pi/2 < \phi < \pi/2$.

When the temperature is further increased to $kT \gg \hbar v_F/l$ this periodic structure is smeared out and the IVC once again becomes a straight line, but with renormalized slope. In this high-temperature limit the amplitude of the terms in the sum in Eq. (52) oscillates with a period $\hbar v_F/l$. During this period, the filling factors n can be taken to be constant, and we can sum over one period to get the average value. Performing this summation in the continuum limit, we get

$$\begin{aligned} & \sum_{\text{one period}} \frac{\cos \chi - \cos \phi}{1 - (D \cos \phi + R \cos \chi)^2} \\ & \approx \frac{\hbar v_F}{2l} \int_0^{2\pi} \frac{\cos(\chi) - \cos(\phi)}{1 - (D \cos \phi + R \cos \chi)^2} d\chi \\ & = \frac{L}{l} \frac{1}{8R\sqrt{D}} \left(\frac{|\sin(\phi/2)|}{\sqrt{1-D\cos^2(\phi/2)}} - \frac{|\cos(\phi/2)|}{\sqrt{1-D\sin^2(\phi/2)}} \right). \end{aligned} \quad (53)$$

This quantity is energy independent and we can then sum over the filling factors following the procedure from the symmetric case (49):

$$\sum_{\text{averaged periods}} (n^e - n^h) \approx \frac{4l}{\hbar v_F \pi} f(V, T). \quad (54)$$

The anomalous current then becomes

$$\begin{aligned} I_a & = -\sigma 2 \frac{e}{\hbar} \frac{D}{\pi \sqrt{R}} \sin \phi \\ & \times \left(\frac{|\sin(\phi/2)|}{\sqrt{1-D\cos^2(\phi/2)}} - \frac{|\cos(\phi/2)|}{\sqrt{1-D\sin^2(\phi/2)}} \right) f(V, T), \end{aligned} \quad (55)$$

which is independent of both the length L and the asymmetry l . We also find that the renormalized anomalous current becomes π periodic. This can qualitatively be explained by the fact that the 2π -periodic part of the anomalous current density is very sensitive to asymmetry, oscillating fast with energy on the scale of $\hbar v_F/l$, becoming washed out during summation over bound states at high temperatures kT

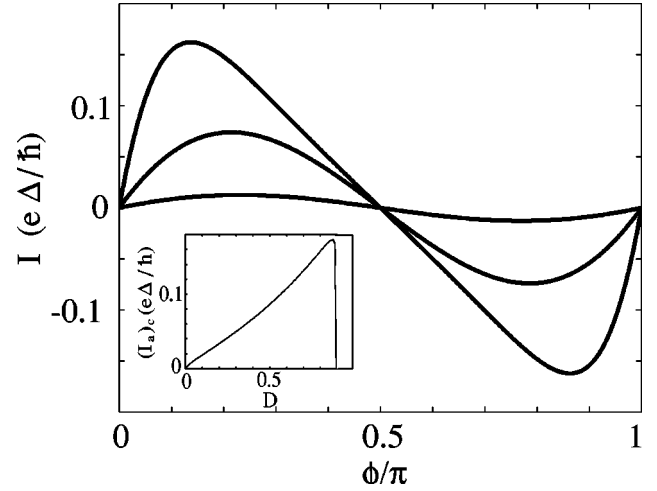


FIG. 11. The asymmetric anomalous current I_a at $eV=\Delta$ and $kT \gg \hbar v_F/L$ as a function of phase difference ϕ for different transparencies $D=0.1, 0.5$, and 0.9 . Inset: The critical anomalous current $(I_a)_c$, for $eV=\Delta$ and $kT \gg \hbar v_F/L$, as a function of transparency D for coupling constant $\epsilon=0.1$.

$\gg \hbar v_F/l$. The π periodic part of the current does not have this sensitivity and is the only part of the anomalous current that survives. The asymmetric anomalous current-phase relation is shown in Fig. 11.

The π periodicity and the zeros at $\phi=n\pi/2$ give the condition that the slope of the IVC must change sign due to asymmetry in the range $-\pi/2 < \phi < \pi/2$, as shown in Fig. 10. The critical asymmetric anomalous current as a function of transparency D is shown in the inset in Fig. 11. The behavior is very similar to the critical anomalous current in the symmetric case, the main difference being that the amplitude is reduced by roughly a factor of 2.

VI. INTERFACE BARRIERS

In any realistic experimental situation, normal reflection at the NS interface, modeled by a barrier with reflection amplitude r_b , must be taken into account.³³ The general expression, considering both the interface barriers and the midpoint scatterer, becomes analytically intractable. We can however analyze the case where the midpoint scatterer is absent ($R=0$) to get an understanding of the effect of NS barriers on the junction properties, and then treat the general case with injection and midpoint scatterer numerically.

In the absence of the superconducting leads (a NININ junction), the two barriers give rise to normal Breit-Wigner resonances for the electrons and holes. Understating the properties of these resonances turns out to be crucial for describing the behavior of Andreev levels and current transport. The energies of the electron and hole resonances are calculated straightforwardly:

$$\begin{aligned} E_n^e & = -2E_F \left[1 - \frac{\pi(n-\nu)}{k_F L} \right], \\ E_m^h & = 2E_F \left[1 - \frac{\pi(m-\nu)}{k_F L} \right], \end{aligned} \quad (56)$$

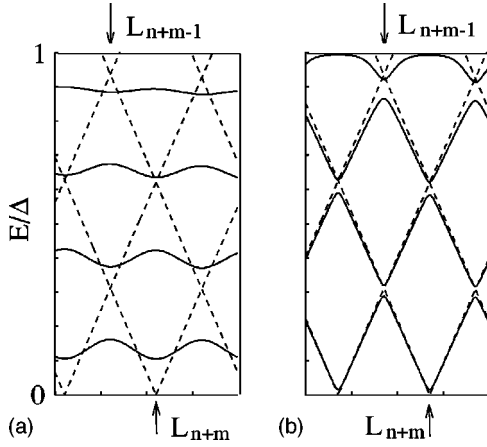


FIG. 12. The Andreev levels (solid) and the normal electron and hole resonances (dotted) as a function of length L of the junction with four Andreev levels in (a) weak resonance limit $R_b \ll 1$ (b) strong resonance limit $R_b \sim 1$. The lengths of two subsequent intersections of normal resonances L_{n+m} and L_{n+m-1} are shown with arrows.

where $r_b = \sqrt{R_b} e^{i\nu\pi}$ and $n(m)$ are integers denoting the index of the electron (hole) resonances. The intersection between electron and hole resonances ($E_n^e = E_m^h$) is given by $L_{n+m} = \lambda_F/4(m+n-2\nu)$ with the Fermi wavelength $\lambda_F = 2\pi/k_F$. These normal resonances are plotted in Fig. 12.

For the junction with superconducting leads, one can in the same way as before calculate the equation for the bound Andreev states ($|E| < \Delta$), with the result³⁵

$$D_b^2 \cos \phi + 2R_b \cos \beta - \cos(2\gamma - \beta) - R_b^2 \cos(2\gamma + \beta) - 4R_b \sin^2 \gamma \cos(\beta_0) = 0, \quad (57)$$

where we have defined $\beta_0 = \pm 2E^{e,h}/(\hbar v_F/L)$ and $+$ ($-$) denotes hole (electron) resonance energies. One can draw some qualitative conclusions on how the Andreev levels are related to the normal resonances by looking at Fig. 12. In the limit of high barrier transparency $R_b \ll 1$, the Andreev levels are weakly modified by the barriers. In the opposite limit $R_b \sim 1$, the Andreev levels get pinned at the normal resonances, but there are no level crossings at the points where the normal electron and hole resonances intersect.

We find the same interlevel distance $\hbar v_F \pi/L$ in the junction with the superconducting leads (SINIS junction) and normal leads (NININ junction). The main difference is that the normal resonance move very quickly through the junction when the length L increases, while the Andreev levels oscillate up and down.

Considering Andreev state energies close to the Fermi level, $E \ll \Delta$, one can derive a simplified dispersion relation,³⁴

$$\sin^2(\beta/2) = \frac{D_b^2 \cos^2(\phi/2) + 4R_b \sin^2(\beta_0/2)}{(1+R_b)^2}. \quad (58)$$

Using this relation we can study the bound state current in different length limits.

In the short limit, $L \ll \xi_0$ there are two cases to be considered. For nearly transparent barriers $D_b \sim 1$, and thus broad resonances $\Gamma = D_b \hbar v_F/L \gg \Delta$, one can neglect dephasing

(putting $\beta = 0$) and just get the total transparency of the junction $D = D_b^2/[D_b^2 + 4R_b \sin^2(\beta_0/2)]$ to be put into the standard zero length junction equilibrium current formula. In the strong barrier case $D_b \ll 1$ the resonances are sharp $\Gamma \ll \Delta$ and one can not neglect the dephasing. Assuming that the resonance is close to Fermi energy $E^{e,h} \ll \Delta$, we can put $\beta \ll 1$ in Eq. (58) and obtain^{35,36}

$$E = \pm \sqrt{\Gamma^2 \cos^2(\phi/2) + (E^{e,h})^2}. \quad (59)$$

When the resonance is exactly at the Fermi energy $E^{e,h} = 0$, the Josephson current is given by

$$I = \frac{e\Gamma}{\hbar} \sin(\phi/2) \tanh\left(\frac{\Gamma \cos(\phi/2)}{2kT}\right). \quad (60)$$

The critical current at low temperatures ($kT \ll \Gamma$) is thus smaller than the critical current of a short, clean junction by a factor Γ/Δ .

For a long junction $L \gg \xi_0$ we can calculate the derivative of energy with respect to phase,

$$\frac{dE}{d\phi} = \pm \frac{\hbar v_F}{2L} \frac{D_b^2 \sin \phi}{\sqrt{(1+R_b)^4 - [D_b \cos \phi - 4R_b \cos(\beta_0)]^2}}, \quad (61)$$

In the weak barrier limit $R_b \ll 1$, this just causes oscillations with length around the clean junction ($R_b = 0$) result. In the strong barrier limit $R_b \sim 1$, one can distinguish two limits: When the length of the junction is far away from the length L_{n+m} where the electron and hole resonances intersect, the junction is out of resonance. The second term in Eq. (61) is negligible and the current from the individual levels thus becomes

$$I = \pm \frac{e v_F}{4L} D_b^2 \sin \phi. \quad (62)$$

It is proportional to D_b^2 and thus strongly suppressed. In the opposite limit, when the length of the junction $L = L_{n+m} = \lambda_F(m+n-2\nu)/4$, the junction is in resonance. When $n+m$ is even we get the current carried by each level

$$I = \pm \frac{e v_F}{L} \frac{D_b \sin \phi}{4|\cos(\phi/2)|} \quad (63)$$

and when $n+m$ is odd we get

$$I = \pm \frac{e v_F}{L} \frac{D_b \sin \phi}{4|\sin(\phi/2)|}. \quad (64)$$

We see that the current is proportional to D_b , just as expected for the junction in resonance. The current carried is thus of the order of the single barrier junction current. An interesting feature is that the current is dependent on the parity of the sum of the electron and hole resonance indices $n+m$. When the third lead is connected to the junction, the scattering at the connection point just splits the Breit-Wigner resonances, and the qualitative picture for the bound states derived without the third lead connected survives.

To calculate the total equilibrium, regular or anomalous current, the currents carried by all individual levels have to be summed up. In the weak barrier limit $R_b \ll 1$ we just find

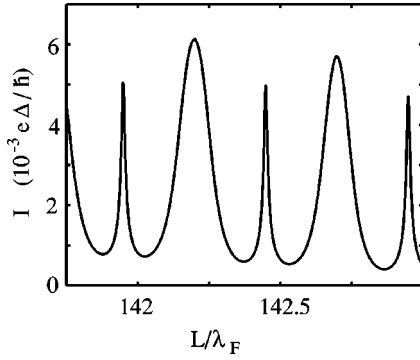


FIG. 13. Short segment of the equilibrium bound state current as a function of length L , to illustrate the resonant behavior. The junction is long $L \gg \xi_0$ with $R_b = 0.9$, $\epsilon = 0.01$ and $\phi = \pi/2$.

that all properties calculated above for the symmetric junction without barriers hold, with a small length dependent modulation $\sim R_b$ with a period $\delta L \sim \lambda_F$. In the strong barrier limit $R_b \sim 1$, the result will depend on whether the junction is in or out of resonance.

Figure 13 shows the resonant behavior of the equilibrium current as a function of length. The current has a peak around lengths $L = \lambda_F/4(m + n + 2\nu)$. The phase dependence of the current at the resonant peaks is well described by the expressions for the single level currents (63) and (64).

The anomalous current is also strongly length dependent and when the junction is in resonance we have an anomalous current $I_a \sim \sigma D_b \sqrt{RD}$ while when we are out of resonance $I_a \sim \sigma D_b^2 \sqrt{RD}$. It turns out that there is an anomalous current even without scattering at the connection point, but it oscillates around zero as a function of length with the period $\sim \lambda_F$.

VII. INJECTION CURRENT

In this section, we turn to a discussion of the injection current. This current is small within our assumption of $\epsilon \ll 1$; however, in practice, it may be comparable to the Josephson current and therefore important for the nonequilibrium Josephson effect as was explained in the Introduction and in Sec. II. The injection current can also be used for experimental detection of the nonequilibrium Josephson current.^{16,37} This current has a close microscopic relation to the anomalous Josephson current.

Although there is a large amount of literature on the normal conducting properties of SNS structures,³⁸ starting with the pioneering work by Spivak and Khmel'nitskii³⁹ and Altshuler, Khmel'nitskii, and Spivak⁴⁰, most of the work is devoted to diffusive junctions. Quantum junctions have quantitatively different properties, but have received much less attention. However, as we will see, many phenomena found in diffusive junctions also exist in quantum junctions and they can qualitatively be explained within our simple and physically intuitive model.

A. Symmetric injection

We start by discussing symmetric junctions, $l=0$. It follows from a straightforward comparison of Eqs. (18) and

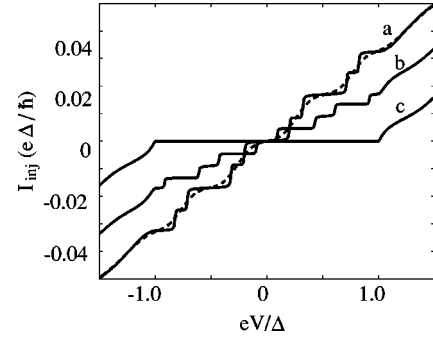


FIG. 14. The injection current in lead 1 as a function of voltage for (a) $\phi = \pi/4$, (b) $\phi = 3\pi/4$, and (c) $\phi = \pi$. Zero T (solid lines) and $T = 0.05\Delta$ (dashed line) with $D = 0.8$, $L = 10\xi_0$, and $\epsilon = 0.05$. For $eV > \Delta$ the slope of the IVC approaches the value of a normal junction.

(19) that the injection and anomalous Josephson currents at $eV < \Delta$ are connected in this case by a simple relation,

$$I_{inj} = -\sigma \frac{\epsilon}{\sqrt{RD - \epsilon^2/4}} \frac{1 + \cos \phi}{\sin \phi} I_a. \quad (65)$$

Therefore the injection current increases stepwise with applied voltage at low temperature just as the anomalous current (see Fig. 14). However, for $eV > \Delta$ the injection current continues to grow, unlike the anomalous Josephson current, which saturates for $eV > \Delta$ (see Sec. V C). In this voltage regime, the injection current steps turn to smooth oscillations, due to the broadening of resonances, around a straight line with the slope corresponding to the normal conductance $G_N = 4\epsilon e^2/h$ [see Eq. (A3)]. The amplitude of the oscillations decreases with increased voltage.

We now focus on the properties of the injection current at subgap voltages $eV < \Delta$. An explicit expression for this current²¹ is given by inserting Eq. (19) into Eq. (31),

$$I_{inj} = \epsilon^2 \frac{4e^2}{h} \int_{-\Delta}^{\Delta} dE (n_e - n_h) \times \frac{2 \cos^2(\phi/2) \sin^2 \theta}{[(1 - \epsilon) \cos 2\theta - R - D \cos \phi]^2 + \epsilon^2 \sin^2 2\theta}. \quad (66)$$

The height and position of the current steps are strongly dependent on the length of the junction. The height of the steps is most conveniently calculated in the weak coupling limit, where the general current expression in Eq. (66) is given by

$$I_{inj} = \epsilon \frac{e}{h} \frac{|\cos(\phi/2)|}{\sqrt{D} \sqrt{1 - D \sin^2(\phi/2)}} \times \sum_{n,\pm} \left| \frac{dE_n^\pm}{d\phi} \right| [n^e(E_n^\pm) - n^h(E_n^\pm)]. \quad (67)$$

In the limit of zero length of the junction (single Andreev level) the magnitude of the step at zero temperature is

$$\delta I_{inj} = \epsilon \frac{e}{\hbar} \frac{\sqrt{D}}{2} \frac{|\sin(\phi/2)| \cos^2(\phi/2)}{1 - D \sin^2(\phi/2)}, \quad (68)$$

while for two levels in junctions of finite length, $L \sim \xi_0$, the steps are

$$\delta I_{inj} = \epsilon \frac{e \Delta}{\hbar} \frac{L}{\xi_0} \frac{\cos^2(\phi/2)}{\sqrt{1 - D \sin^2(\phi/2)}} \quad (69)$$

($E_0^\pm \approx \Delta$). For long junctions $L \gg \xi_0$, the current step is

$$\delta I_{inj} = \epsilon \frac{e}{\hbar} \frac{\hbar v_F}{L} \frac{\cos^2(\phi/2)}{1 - D \sin^2(\phi/2)}. \quad (70)$$

There are some features of the current, which are independent of the length of the junction. The maximum magnitude of the differential conductance dI_{inj}/dV at the current onsets is independent of ϵ and equal to $4e^2/h$; this property has been noticed in Ref. 15. At the same time, the maximum magnitude of the conductance at the current plateaus is a factor of ϵ^2 smaller. Therefore the amplitude of the current-phase oscillations strongly varies with voltage and also with junction parameters, e.g., junction transmissivity D . For example, in junctions with finite transmissivity $D \neq 1$, there is a current plateau at zero voltage and therefore the amplitude of the current-phase oscillations is small, while it dramatically increases at $D = 1$ when the Andreev resonance approaches the Fermi level. This giant enhancement of the conductance oscillations has been discussed by Kadigrobov *et al.*²²

There is a π shift of the conductance oscillations as a function of phase when moving from one current plateau to another. Such a crossover has been found by Leadbeater and Lambert⁴¹ by numerical simulations of multimode SNS junctions with arbitrary impurity concentration. In the diffusive limit, a similar phenomenon, π shift of the conductance oscillations when the voltage passes the Thouless energy, has been discussed by Volkov and Zaitsev.⁴² This effect has been experimentally observed in various structures.^{43–45} Within our model, the crossover phenomenon has a very simple explanation which follows from the phase dependence of the Andreev resonances presented in Fig. 4. At a given voltage, the magnitude of the conductance depends on the distance to the nearest Andreev resonance: the closer the resonance the bigger the conductance. As is clear from the figure, when the phase difference changes from zero to π , the distance between the Andreev resonances confining the odd current plateaus (the first plateau is at zero voltage) decreases, while the distance between the resonances confining the even plateaus increases. As a result, the conductance at the odd plateaus has a maximum around π , while the conductance at the even plateaus has a maximum at zero phase difference. Similar arguments hold for the phase dependence of the conductance in diffusive junctions below and above the Thouless energy, which plays the role of the first Andreev resonance. The conductance as a function of phase for different voltages is plotted in Fig. 15.

At finite temperature, the step structure in the IVC in Fig. 14 is smeared. This effect is most interesting in long junctions, where the temperature can be much larger than the distance between the Andreev levels, $kT \gg \hbar v_F/L$ without suppressing superconductivity itself, $kT \ll \Delta$. The expression

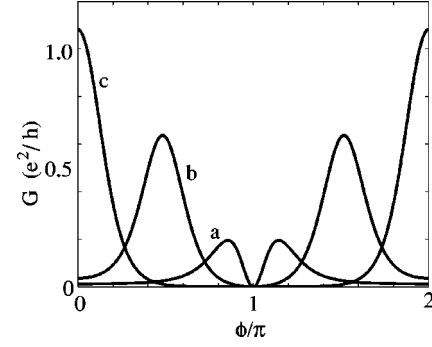


FIG. 15. The conductance as a function of ϕ for different voltages (a) $eV=0$, (b) $eV=0.075\Delta$, and (c) $eV=0.15\Delta$ at zero temperature $T=0$. $D=0.9$, $\epsilon=0.05$, and $L=20\xi_0$. The conductance maximum shifts from $\phi \approx \pi$ to $\phi=0$ upon increasing voltage. There is an absolute minimum at $\phi=\pi$.

for the current in this temperature limit is obtained by inserting Eq. (41) into Eq. (67) and then converting the sum over Andreev levels into an integral, just as for the anomalous current, see Eq. (49). The current is then given by

$$I_{inj} = \epsilon \frac{4e}{h} \frac{\cos^2(\phi/2)}{1 - D \sin^2(\phi/2)} f(V, T), \quad (71)$$

where $f(V, T)$ is given by Eq. (50). The IVC becomes linear for $eV < \Delta$, with the slope independent of the length of the junction and the temperature. The current is thus a true long-range current. From Eq. (71) it is clear that the conductance has a maximum at $\phi=0$ and a minimum at $\phi=\pi$ for all applied voltages $eV < \Delta$. This is different from the phase dependence of the conductance at odd current plateaus at zero temperature, and therefore at these plateaus the current-phase oscillations undergoes a π shift as a function of temperature at $kT \sim \hbar v_F/L$. The conductance as a function of phase difference is plotted for different temperatures in the inset in Fig. 16. Such a crossover has recently been observed in quasiballistic junctions by Dimoulas *et al.*⁴³ and also a similar crossover has been observed in diffusive junctions at the Thouless temperature.⁴⁶

It is interesting to point out that the information on the conductance as a function of phase difference was used recently by Baselmans *et al.*⁶ to determine the direction of the Josephson current. In a loop geometry a large current circulating in the loop may change the applied external flux vs phase dependence, thus modifying the phase dependence of the conductance.³⁷

When discussing symmetric junctions, it is also worth noting that the effect discussed by Volkov and Pavlovskii¹⁹ does not exist in these junctions because the injection current is equally distributed between the left and the right arms of the junction [see Eq. (20)].

B. Asymmetric injection

The effect of asymmetry on the injection current is most drastic in the limit of a long junction with large asymmetry $L \gg l \gg \xi_0$, just as for the asymmetric anomalous current. This shows the strong relationship between the two currents. The injection current is given by inserting Eq. (26) into Eq. (31)

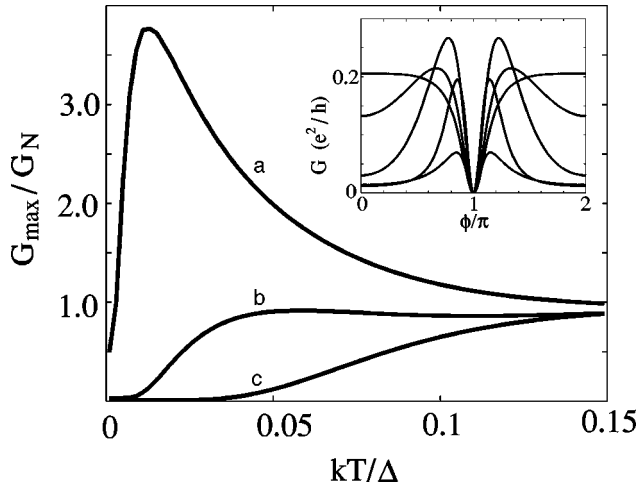


FIG. 16. The maximum conductance G_{max}/G_N as a function of T for zero voltage for different junction transparencies, (a) $D=0.94$, (b) $D=0.9$, and (c) $D=0.1$ and $\epsilon=0.01$. The maximum conductance saturates at a constant value $G_{max}=G_N$ for $kT \gg \hbar v_F/L$, independent on D . Inset: The conductance as a function of ϕ for different temperatures $kT=0, 0.01\Delta, 0.025\Delta, 0.05\Delta$, and 0.1Δ at zero voltage $V=0$. Increasing temperature from bottom to top at $\phi=0$. $D=0.9$, $\epsilon=0.05$, and $L=20\xi_0$.

$$I_{inj} = \epsilon \frac{e \hbar v_F}{\hbar L} \sum_{n=0}^N \frac{D \sin^2(\phi) + R \sin^2 \chi}{1 - (D \cos \phi + R \cos \chi)^2} (n^e - n^h). \quad (72)$$

Averaging over periods and summing up the filling factors, just as in the case of the anomalous current [see Eq. (53)], the injection current becomes

$$I_{inj} = \epsilon \frac{e}{\hbar} \frac{8}{R\pi} \left[1 - \sqrt{D} \times \left(\frac{|\sin(\phi/2)|^3}{\sqrt{1 - D \cos^2(\phi/2)}} + \frac{|\cos(\phi/2)|^3}{\sqrt{1 - D \sin^2(\phi/2)}} \right) \right] f(V, T). \quad (73)$$

The injection current in this limit does not depend on either the length L or the asymmetry l . It is π periodic, $I_{inj}(\phi + \pi) = I_{inj}(\phi)$, and this property can be qualitatively explained by considering the lowest order paths giving rise to the current.

The upper paths in Fig. 17, corresponding to an injected electron and giving rise to an outgoing hole, produce a current of the order $i_{inj} \sim |e^{i(\phi_L + \beta_2)} + e^{i(\phi_R + \beta_3)}|^2 = 2 + 2 \cos(\phi + \chi)$. This part of the current is 2π periodic in the phase, oscillating in energy with a period $\hbar v_F/l$. It is washed out when summing up the levels in a long junction at temperatures $kT \gg \hbar v_F/l$. The lower paths in Fig. 17, corresponding to an injected electron giving rise to an outgoing electron, produce a current of the order $i_{inj} \sim |d^* e^{i(\phi + \beta)} + d e^{i(-\phi + \beta)}|^2 = D(2 + 2 \cos 2\phi)$. This part of the current is π periodic in phase and not sensitive to asymmetry.

The discussion about the periodicity of the conductance oscillations with respect to phase goes back to the early eighties. A π -periodic contribution to the weak localization correction to the conductance in a SNS junction was pre-

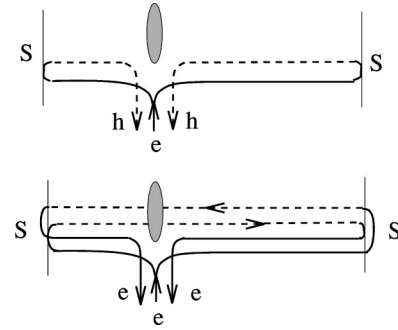


FIG. 17. The paths in the asymmetric junction giving the first-order terms of the current. Electrons are drawn with solid lines, holes with dashed. The gray ellipse denotes the effective scatterer due to the three-lead connection. The upper paths give rise to a 2π periodic component of the current, suppressed at finite temperature $kT \gg \hbar v_F/L$. The lower paths, time reversed, give rise to a π periodic component of the current, not suppressed by temperature.

dicted by Spivak and Khmelnitskii³⁹ and later Altshuler, Khmelnitskii, and Spivak⁴⁰. It has been shown in numerical simulations for a structure similar to ours that the full conductance, i.e., not only the weak localization contribution, might become π periodic at finite temperatures.⁴⁷ A large π -periodic conductance oscillation with phase was also observed in diffusive samples.⁴⁸ Whether the explanation for the crossover from 2π to π periodicity with increased temperature discussed above can account for these observations remains to be investigated.

VIII. FOUR-TERMINAL JUNCTIONS

The basic properties of the nonequilibrium Josephson current do not change when connecting a second normal reservoir to the normal part of the junction. However, the injection current becomes qualitatively different due to additional interference between injected quasiparticles that undergo Andreev reflections and quasiparticles that only scatter normally.

A. Josephson current

Due to the additional normal electron reservoir, four-terminal junctions can be biased in different ways. Two types of junction configurations are used in experiments.^{6,49} The junction (a) in Fig. 18 is a straightforward extension of the three terminal device pictured in Fig. 1. Two normal reservoirs are connected to the normal part of the junction. The reservoirs are then connected to the grounded superconducting loop via voltage sources biased at V_1 and V_4 , respectively. In the general case, the currents I_1 and I_4 are not equal and thus $I_2 \neq I_3$.

In the junction (b) in Fig. 1, a bias V is applied between the two normal reservoirs, which are only connected to the superconducting loop via the four-lead connection point. In this case it follows from current conservation that $I_2 = I_3$. This junction reduces to the junction (a) in Fig. 1 by defining the potential of the superconducting loop be zero and determining the potentials V_1 and $V_4 = V_1 - V$ self-consistently from the current conservation condition $I_1(V_1, V_4) = I_4(V_1, V_4)$.

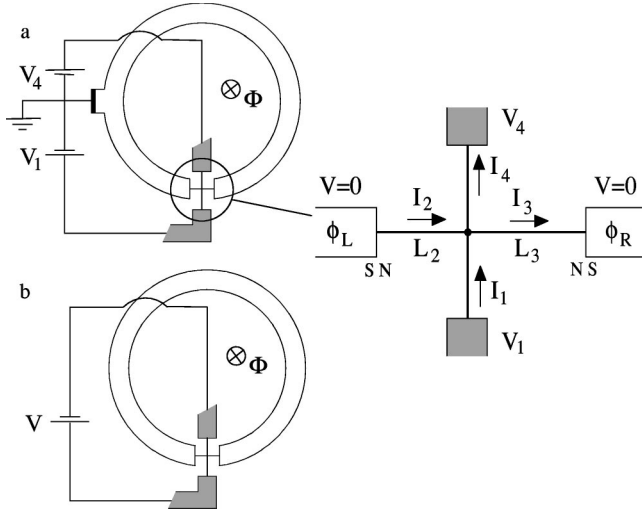


FIG. 18. Two different setups of the four terminal junction. In (a) the normal reservoirs are biased independently at V_1 and V_4 with respect to the superconducting loop (grounded), in (b) only the potential difference between the normal reservoirs, V , is determined. In the right figure, a close up of the junction area is shown, with the direction of the currents showed with arrows

The cross-shaped connection point is modeled for simplicity by the symmetric scattering matrix

$$S = \begin{pmatrix} r_{\perp} & \sqrt{\epsilon} & \sqrt{\epsilon} & d_{\perp} \\ \sqrt{\epsilon} & r & d & \sqrt{\epsilon} \\ \sqrt{\epsilon} & d & r & \sqrt{\epsilon} \\ d_{\perp} & \sqrt{\epsilon} & \sqrt{\epsilon} & r_{\perp} \end{pmatrix}, \quad (74)$$

where ϵ describes the coupling of the SNS junction to the vertical normal leads ($0 \leq \epsilon \leq 0.25$). The horizontal scattering amplitudes now obey the relations $\text{Re}(rd^*) = -\epsilon$ and $D+R=1-2\epsilon$. The same holds for the vertical scattering amplitudes r_{\perp} and d_{\perp} .

The current densities $i_j^{e(h),1(4)}$, with the upper index 1 or 4 denoting the lead from which the quasiparticles are injected, are calculated in the same way as in the case of the three terminal junction. Due to the symmetry of the scattering matrix, quasiparticles injected from leads 1 or 4 give rise to the same current density in leads 2 and 3, i.e., $i_2^{e(h),1} = i_2^{e(h),4}$ and $i_3^{e(h),1} = i_3^{e(h),4}$.

The expressions for the sum and difference current densities in leads 2 and 3 become very similar to the three terminal expressions [see Eqs. (17)–(19)], one just changes $\epsilon \rightarrow 2\epsilon$ and divides by 2. Neither the vertical transparency D_{\perp} nor the reflectivity R_{\perp} thus appear explicitly in these expressions. In the limit of weak coupling $\epsilon \ll 1$, $i^{+,1} = i^{+,4} = i^{+}/2$ and $i_a^1 = i_a^4 = i_a/2$, and the Josephson current is therefore given by the equation

$$I = I_{eq} + \frac{1}{2}[I_r(V_1) + I_r(V_4)] + \frac{1}{2}[I_a(V_1) + I_a(V_4)], \quad (75)$$

where the currents I_{eq} , I_r and I_a are the same as in the three terminal case, Eqs. (33)–(35). Noting the relations $I_r(-V)$

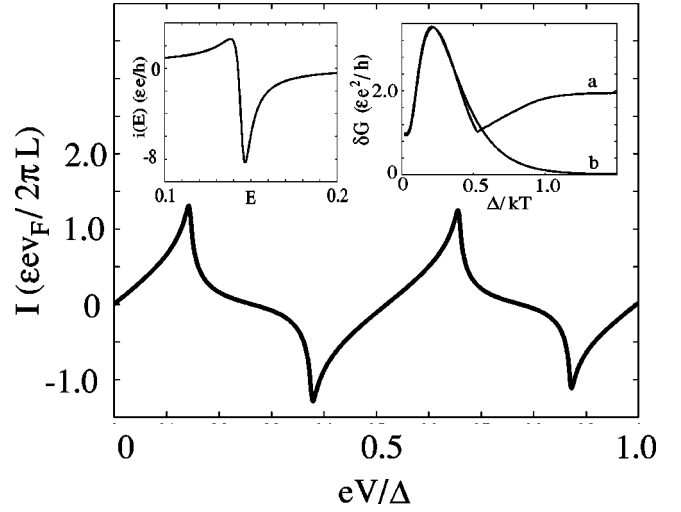


FIG. 19. The interference part of the injection current as a function of voltage $V = V_1 = -V_4$ for zero temperature. The junction parameters are $\phi = \pi/2$, $L = 10\xi_0$, $D_{\perp} = 0.6$, $D = 0.8$, and $\epsilon = 0.02$. Left inset: The current density $i(E)$ for the first resonance at $E \approx 0.14\Delta$. Right inset, the zero voltage conductance as function of temperature for two different bias arrangements (a) $V_1 = V$ and $V_4 = 0$, and (b) $V_1 = -V_4 = V$ for $D_{\perp} = 0.01$, $D = 0.8$, $\epsilon = 0.01$ and $L = 20\xi_0$.

$= I_r(V)$ and $I_a(-V) = -I_a(V)$, we see that for bias $V_1 + V_4 = 0$ the anomalous current is zero, and for $V_1 - V_4 = 0$ the regular current is zero.

B. Injection current

For the injection current, we only consider the case of symmetric junction, $l=0$, and no barriers at the NS interfaces. In this case, the part of the injection current that flows into the horizontal leads 2 and 3 of the junction is symmetrically split between the leads. The subgap current can be written on the form

$$I_{1(4)} = I_{direct}(V_1 - V_4) \pm \frac{I'_{inj}(V_1) + I'_{inj}(V_4)}{2} + I_{int} \quad (76)$$

(detailed expressions are presented in Appendix D). The first term is the current flowing directly between the reservoirs,

$$I_{direct} = (2e/h)(D_{\perp} + \epsilon)(V_1 - V_4), \quad (77)$$

while the second term I'_{inj} differs from the three-terminal injection current in Eq. (66) by changing $\epsilon \rightarrow 2\epsilon$. These two terms can be understood as a straightforward extension of the three terminal injection current. The sum of these two terms reduce to the normal current expression $I_{1(4)} = (2e/h)[(D_{\perp} + \epsilon)(V_1 - V_4) \pm \epsilon(V_1 + V_4)]$ in the case when the junction is normal.

The last current term I_{int} in Eq. (76), however, does not exist in the three-terminal junctions. It arises from the interference between quasiparticles being reflected or transmitted in the vertical leads and quasiparticles forming the Andreev resonance by multiple scattering in the horizontal leads. This interference leads to a new type of resonances, Fano resonances,⁵⁰ which are situated at the same energy as the Andreev resonances (see left inset in Fig. 19). The Fano

resonances in the current density give rise to a current I_{int} periodically oscillating around zero (rather than stepwise growing) as a function of applied voltage and having sharp peaks, as shown on Fig. 19, the height of the peaks of the order of $\epsilon \ln \epsilon$. For bias voltages between the resonances, the conductance is of the order of ϵ , which is much larger than the conductance at the current plateaus for the three-terminal junctions, $\sim \epsilon^2$. It is interesting to mention that the interference current does not turn to zero at $\phi = \pi$, in contrast to the three-terminal injection current [see Eq. (D3)]. The current I_{int} is plotted in Fig. 19 for a particularly interesting bias arrangement, $V_1 = -V_4 = V$, when the second term in Eq. (76) disappears due to the symmetry relation $I_{inj}(-V) = -I_{inj}(V)$ [see Eq. (66)], and the interference current I_{int} fully accounts for the current oscillations with voltage and superconducting phase.

With increasing temperature, the oscillations of the interference current are suppressed and disappear completely at temperatures larger than the distance between the resonances, $kT \gg \hbar v_F / L$. Thus the amplitude of the oscillations of the total current in this limit approaches zero if $V_1 = -V_4$, while it remains finite in the general case, $V_1 \neq -V_4$, due to oscillations of the current I_{inj} . This is shown in the right inset in Fig. 19, where the amplitude of the conductance oscillations with the phase difference at zero voltage, $\delta G = G_{max} - G_{min}$ is plotted as a function of temperature. In the temperature interval $\hbar v_F / L \ll kT \ll \Delta$, the total current of a long junction is independent of temperature and length of the junction and obeys the equation

$$I_{1(4)} = \frac{2e^2}{h} \left[(D_{\perp} + \epsilon)(V_1 - V_4) \pm \epsilon \frac{\cos^2(\phi/2)}{1 - D \sin^2 \phi/2} \times (V_1 + V_4) \right]. \quad (78)$$

It follows from this equation that the differential conductance dI_1/dV_1 (and dI_4/dV_4) is always smaller than (or equal to, for $\phi = 0$) the conductance of the normal junction $G_N = 2e^2/h(D_{\perp} + 2\epsilon)$. The effect of superconductivity in this temperature regime is thus always to *decrease* the conductance.

IX. CONCLUSIONS

We have presented a detailed study of the nonequilibrium Josephson effect in quantum three- and four-terminal SNS-devices. A prominent feature of open nonequilibrium quantum SNS structures is the anomalous dc Josephson current. This current results from a modification of the current carrying Andreev states in the SNS junction, due to connection of the junction to a normal electron reservoir. The anomalous current is revealed under nonequilibrium conditions created by applying a voltage between the normal reservoir and the SNS junction. The anomalous Josephson current is sensitive to the scattering phase shift at the injection point while other junction properties (asymmetric position of the injection point, transmissivity of the injector and NS interfaces) do not qualitatively affect the current. The current grows with applied voltage and saturates at $eV > \Delta$ at a magnitude corresponding to the current of a short junction, with critical cur-

rent $I_c \sim e\Delta\sqrt{D}/\hbar$ independent on the junction length. This enhancement of the critical current persists even in the long junction limit $L \gg \xi_T$. Such behavior is in sharp contrast to the effect of nonequilibrium population of the Andreev states, which merely induces oscillations and sign reversal of the Josephson current as a function of applied injection voltage. The enhancement of the critical current in this case is strongly length dependent: at best it can be as big as $I_c \sim 1/L$ at $eV > \Delta$ in long junctions and it decays with the junction length.

The long-range effect in the anomalous Josephson current is microscopically connected to the similar property of the injection current: the injection current oscillates with the superconducting phase difference (exhibiting full-scale oscillation for symmetric injection in a three-terminal junctions, with zero at $\phi = \pi$), with the amplitude of the oscillation not depending on the junction length.

The current-voltage characteristics of both the Josephson and injection currents have pronounced steplike features, due to the effect of Andreev resonances, with the position and height of the current features strongly dependent on the superconducting phase difference. These features are washed out by temperature. In long junctions with asymmetric injection the superconducting phase dependence of the temperature-smearred current-voltage characteristics becomes π periodic. In the presence of electron back scattering at the NS interfaces, the current oscillates strongly as a function of the junction length due to the effect of normal electron Breit-Wigner resonances. The Josephson effect is qualitatively similar in three- and four-terminal junctions, while the injection current in four-terminal junctions exhibits a specific resonant behavior due to Fano resonances.

ACKNOWLEDGMENTS

This work has been supported by research grants from NFR, TFR, NUTEK (Sweden), and by a NEDO International Joint Research Grant (Japan).

APPENDIX A: CONTINUUM STATE CURRENT

Here we present formulas for the continuum current for a symmetric ($l=0$) three-terminal junction without barriers at the NS interfaces. The continuum current consists of particles injected from both the normal reservoir and the superconducting reservoirs. The current density in lead 2 from all injected quasiparticles from the superconductors is

$$i_2^s = \frac{e}{h} \frac{2 \sin \beta \sinh \gamma_c}{Z_c} \{ \sin \phi [(4D - 2D\epsilon - \epsilon^2) \cosh \gamma_c - 2D\epsilon e^{-\gamma_c}] - 4\sigma\epsilon\sqrt{RD - \epsilon^2} \sin^2(\phi/2) \cosh \gamma_c \}, \quad (A1)$$

where $Z_c = \{ \cos \beta [\cosh 2\gamma_c(1 - \epsilon) + \epsilon \sinh 2\gamma_c] - R - D \cos \phi \}^2 + \{ \sin \beta (\sinh 2\gamma_c(1 - \epsilon) + \epsilon \cosh 2\gamma_c) \}^2$ and $\gamma_c = \text{arccosh}(E/\Delta)$. In lead 3 we get $i_3^s(\phi) = -i_2^s(-\phi)$. This current density is an oscillating function of energy with largest amplitude for energies close to $E = \Delta$ and is given at negative energies by $i_j^s(E) = -i_j^s(-E)$.

For the particles injected from the normal reservoir, the sum current in lead 2 becomes

$$i_2^+ = 2\frac{e}{h} \frac{\epsilon \sin \beta \cosh \gamma_c}{Z_c} \left\{ \sin \phi [2D \cosh \gamma_c + \epsilon \sinh \gamma_c] + 4\sigma \sqrt{RD - \epsilon^2/4} \sin^2(\phi/2) \sinh \gamma_c \right\} \quad (\text{A2})$$

with $i_3^+(\phi) = -i_2^+(-\phi)$ in lead 3. The difference current in lead 2 has the form

$$i_2^- = 2\frac{e}{h} \frac{\epsilon \cosh \gamma_c}{Z_c} \left(-\cosh \gamma_c (\epsilon \cos \phi + 2\sigma \sqrt{RD - \epsilon^2/4} \sin \phi) + (1 - \epsilon) [\sinh \gamma_c - \sinh 3\gamma_c] - \epsilon \cosh 3\gamma_c + \cos \beta \{ 2 \sinh \gamma_c (R + D \cos \phi) + \cosh \gamma_c (\epsilon (1 + \cos \phi) + 2\sigma \sqrt{RD - \epsilon^2/4} \sin \phi) \} \right) \quad (\text{A3})$$

with $i_3^-(\phi) = -i_2^-(-\phi)$ in lead 3. For negative energies we get $i_j^+(E) = -i_j^+(-E)$ and $i_j^-(E) = i_j^-(-E)$.

In the limit of weak coupling, $i_2^s = i_3^s = i^s$ and the total continuum current is given by, inserting Eq. (A1) into Eq. (28),

$$I_{eq}^c = \frac{e}{h} \left(\int_{-\infty}^{-\Delta} + \int_{\Delta}^{\infty} \right) dE n_F(E) \times \frac{4D \sin \phi \sin \beta \sinh 2\gamma_c}{(\cos \beta \cosh 2\gamma_c - R - D \cos \phi)^2 + (\sin \beta \sinh 2\gamma_c)^2}. \quad (\text{A4})$$

Following the methods in Ref. 18 one can rewrite this integral as a sum over the residues,

$$I_{eq}^c = -I_{eq}^b + \frac{e}{h} 4kT\pi D \sin \phi \times \sum_{p=0}^{\infty} \left\{ \left[\frac{\omega_p}{\Delta} \cosh \left(\frac{\omega_p L}{\hbar v_F} \right) + \sqrt{1 + \left(\frac{\omega_p}{\Delta} \right)^2} \sinh \left(\frac{\omega_p L}{\hbar v_F} \right) \right]^2 + 1 - D \sin^2(\phi/2) \right\}^{-1}, \quad (\text{A5})$$

where the first term results from the poles of the current density in Eq. (A4) and the second term from the poles at the Matsubara frequencies $\omega_p = 2kT\pi(1/2 + p)$. The first term in Eq. (A5) is the current carried by the bound states with negative sign. The total equilibrium current I_{eq} is then just given by the second term.⁵¹ For $\hbar v_F/L \ll kT \ll \Delta$ only the first term in the sum is important, giving the current in Eq. (44). For $T=0$, the sum over ω is converted to an integral, giving the current in Eq. (43).

APPENDIX B: SPECTRAL DENSITIES OF BOUND STATE CURRENTS

In this appendix we analyze the central quantity in the current density expressions (17)–(19), given by

$$\frac{\epsilon}{Z} = \frac{\epsilon}{[(1 - \epsilon) \cos 2\theta - R \cos \chi - D \cos \phi]^2 + \epsilon^2 \sin^2 2\theta}, \quad (\text{B1})$$

in the limit of zero coupling $\epsilon \rightarrow 0$. We can conveniently rewrite

$$\frac{\epsilon}{Z} = \frac{1}{\sin^2 2\theta} \frac{\epsilon}{F^2 + \epsilon^2} \quad (\text{B2})$$

with $F(E, \phi) = [(1 - \epsilon) \cos 2\theta - R \cos \chi - D \cos \phi] / \sin 2\theta$. In the limit of zero coupling the expression becomes

$$\lim_{\epsilon \rightarrow 0} \frac{\epsilon}{F^2 + \epsilon^2} = \pi \delta(F) = \sum_{n,\pm} \pi \left| \frac{\partial}{\partial E} F \right|^{-1} \delta(E - E_n^\pm) \quad (\text{B3})$$

with the energies E_n^\pm , given by

$$\cos 2\theta - R \cos \chi - D \cos \phi = 0, \quad (\text{B4})$$

being the energies of the bound Andreev states. By rewriting

$$\frac{\partial}{\partial E} F = -\frac{d\phi}{dE} \frac{\partial}{\partial \phi} F = -\frac{d\phi}{dE} \frac{D \sin \phi}{\sin 2\theta} \quad (\text{B5})$$

the expression (B3) becomes

$$\lim_{\epsilon \rightarrow 0} \frac{\epsilon}{Z} = \sum_{n,\pm} \frac{\pi}{D |\sin \phi \sin 2\theta|} \left| \frac{dE}{d\phi} \right| \delta(E - E_n^\pm). \quad (\text{B6})$$

From Eq. (B4), the derivative of energy with respect to phase becomes

$$\frac{dE}{d\phi} = -\frac{D \sin \phi}{2 \sin 2\theta \left(\frac{1}{\sqrt{\Delta^2 - E^2}} + \frac{L}{\hbar v_F} + \frac{l}{\hbar v_F} R \frac{\sin \chi}{\sin 2\theta} \right)}. \quad (\text{B7})$$

Using the relation (B4) and the fact that $R + D = 1$ we can rewrite

$$|\sin 2\theta| = \sqrt{(D + R)^2 - (D \cos \phi + R \cos \chi)^2} = \sqrt{D^2 \sin^2 \phi + R^2 \sin^2 \chi + 2DR(1 - \cos \phi \cos \chi)} \quad (\text{B8})$$

which shows that $|\sin 2\theta| > R |\sin \chi|$. This gives that, since $L \geq l$ by definition, the factor in the parenthesis in the denominator in Eq. (B7) is always positive. The relation

$$\text{sgn} \left(\frac{dE}{d\phi} \sin \phi \sin 2\theta \right) = -1 \quad (\text{B9})$$

then follows from Eq. (B7). Equations (B6) and (B9) are the technical result of this appendix.

APPENDIX C: CURRENTS FOR DIFFERENT JUNCTION LENGTHS

Here we list all expressions for the partial bound state currents in different junction length limits. The junction considered is a symmetric ($l=0$) three terminal junction without

barriers at the NS interfaces, in the weak-coupling limit $\epsilon \ll 1$.

1. Short junction limit ($L \ll \xi_0$)

$$I_{eq}^b = \frac{e\Delta}{\hbar} \frac{D \sin \phi}{2\sqrt{1-D \sin^2(\phi/2)}} \tanh(E_0^-/2kT), \quad (C1)$$

$$I_r = \frac{e\Delta}{\hbar} \frac{D \sin \phi}{4\sqrt{1-D \sin^2(\phi/2)}} g(E_0), \quad (C2)$$

$$I_a = \frac{e}{\hbar} \frac{\sigma D \sqrt{R} \sin \phi |\sin(\phi/2)|}{1-D \sin^2(\phi/2)} h(E_0), \quad (C3)$$

$$I_1 = \frac{e}{\hbar} \frac{\epsilon \sqrt{D} |\sin(\phi/2)|}{1-D \sin^2(\phi/2)} h(E_0). \quad (C4)$$

When there are two Andreev levels, with $1 \ll D$, $\beta/2 > \sqrt{D}$ and $E_0^+ \approx E_0^- \approx \Delta$, the currents become

$$I_{eq}^b = \frac{e\Delta}{\hbar} \frac{L}{\xi_0} \frac{\sqrt{D} \sin(\phi)}{2|\sin(\phi/2)|\sqrt{1-D \sin^2(\phi/2)}} [\tanh(E_0^-/2kT) - \tanh(E_0^+/2kT)], \quad (C5)$$

$$I_r = \frac{e\Delta}{\hbar} \frac{L}{\xi_0} \frac{\sqrt{D} \sin(\phi)}{4|\sin(\phi/2)|\sqrt{1-D \sin^2(\phi/2)}} [g(E_0^+) - g(E_0^-)], \quad (C6)$$

$$I_a = \sigma \frac{e\Delta}{\hbar} \frac{L}{2\xi_0} \frac{\sqrt{RD} \sin \phi}{1-D \sin^2(\phi/2)} [h(E_0^+) + h(E_0^-)], \quad (C7)$$

$$I_1 = \epsilon \frac{e\Delta}{\hbar} \frac{L}{\xi_0} \frac{\cos^2(\phi/2)}{\sqrt{1-D \sin^2(\phi/2)}} [h(E_0^-) + h(E_0^+)]. \quad (C8)$$

2. Long junction limit ($L \gg \xi_0$)

$$I_{eq}^b = \frac{e}{\hbar} \frac{\hbar v_F}{L} \frac{\sqrt{D} \sin(\phi)}{2|\sin(\phi/2)|\sqrt{1-D \sin^2(\phi/2)}} \times \left(\sum_{n=0}^N [\tanh(E_n^-/2kT) - \tanh(E_n^+/2kT)] \right) + i^* \tanh(\Delta/2kT), \quad (C9)$$

$$I_r = \frac{e}{\hbar} \frac{\hbar v_F}{2L} \frac{\sqrt{D} \cos(\phi/2)}{\sqrt{1-D \sin^2(\phi/2)}} \left(\sum_{n=0}^N [g(E_n^-) - g(E_n^+)] \right) + \frac{i^*}{2} g(\Delta), \quad (C10)$$

$$I_a = \frac{e}{\hbar} \frac{\hbar v_F}{L} \frac{\sigma \sqrt{DR} \sin \phi}{2[1-D \sin^2(\phi/2)]} \sum_{n=0}^N [h(E_n^+) + h(E_n^-)], \quad (C11)$$

$$I_1 = \frac{e}{\hbar} \frac{\epsilon \hbar v_F}{2L} \frac{\cos^2(\phi/2)}{1-D \sin^2(\phi/2)} \sum_{n=0}^N [h(E_n^-) + h(E_n^+)], \quad (C12)$$

where

$$h(E) = \tanh[(E - eV)/2kT] - \tanh[(E + eV)/2kT]$$

and

$$g(E) = \tanh[(E + eV)/2kT] + \tanh[(E - eV)/2kT] - 2 \tanh(E/2kT).$$

APPENDIX D: FOUR-TERMINAL INJECTION CURRENT

The full expression for the subgap injection current presented in Eq. (76), is given by using the symmetry relations $i_{1(4)}^{e,1} = -i_{4(1)}^{e,4}$ and $i_{1(4)}^{h,1} = -i_{4(1)}^{h,4}$,

$$I_{1(4)} = \int_{-\infty}^{\infty} dE \frac{e}{\hbar} (D_{\perp} + \epsilon) [n^{e,1} - n^{h,1} - (n^{e,4} - n^{h,4})] \pm i_{inj} [n^{e,1} - n^{h,1} + n^{e,4} - n^{h,4}] + i_0^e [n^{e,1} - n^{e,4}] - i_0^h [n^{h,1} - n^{h,4}]. \quad (D1)$$

The current density i_{inj} is the injection current density in the horizontal leads 2 and 3, given by Eq. (66) when changing $\epsilon \rightarrow 2\epsilon$. The interference current densities are

$$i_0^e = \frac{e}{\hbar} \frac{\epsilon}{Z} \text{Re}\{(r_{\perp} - d_{\perp}) [r + d \cos \phi - (r + d) \exp(i2\theta)] \times (\cos \theta - R - D \cos \phi + i\epsilon 2 \sin 2\theta)\}, \quad (D2)$$

with $i_0^h = -i_0^e(r, d, r_{\perp}, d_{\perp} \rightarrow r^*, d^*, r_{\perp}^*, d_{\perp}^*)$. For a long junction at zero temperature, the interference current in the weak-coupling limit is given by

$$I_{int} = \frac{2e}{\hbar} \epsilon \left\{ (R_{\perp} - D_{\perp}) \left[\frac{\pi \hbar v_F}{4L} \sum_{n,\pm} \Theta(eV - E_n^{\pm}) - V \right] + 2 \frac{\hbar v_F}{L} \frac{\text{Im}(rd^*) \text{Im}(r_{\perp} d_{\perp}^*) |\sin(\phi/2)|}{\sqrt{D} \sqrt{1-D \sin^2(\phi/2)}} \times \ln \left[\frac{\sqrt{1-D \sin^2(\phi/2)} \sin \theta + \sqrt{D} |\sin(\phi/2)| \cos \theta}{\sqrt{1-D \sin^2(\phi/2)} \sin \theta - \sqrt{D} |\sin(\phi/2)| \cos \theta} \right] \right\} \quad (D3)$$

where $V = V_4 = -V_1$ and θ [defined in Eq. (13)] is given at energy $E = eV$. The expression (D3) strictly applies only at $|eV - E_n^{\pm}| \gg \epsilon \hbar v_F / L$. The current at the resonances saturates at magnitude of the order of $\epsilon \ln \epsilon$.

- ¹H. van Houten, Appl. Phys. Lett. **58**, 1326 (1991).
- ²T. Akazaki, H. Takayanagi, and J. Nitta, Appl. Phys. Lett. **68**, 418 (1996).
- ³H. Takayanagi, T. Akazaki, and J. Nitta, Phys. Rev. Lett. **75**, 3533 (1995).
- ⁴Th. Schäpers, J. Malindretos, K. Neurohr, S. Lachenmann, A. van der Hart, G. Crecelius, H. Hardtdegen, H. Lüth, and A.A. Golubov, Appl. Phys. Lett. **73**, 2348 (1998).
- ⁵A.F. Morpurgo, T.M. Klapwijk, and B.J. van Wees, Appl. Phys. Lett. **72**, 966 (1998).
- ⁶J.J.A. Baselmans, A.F. Morpurgo, B.J. van Wees, and T.M. Klapwijk, Nature (London) **397**, 43 (1999).
- ⁷F. Lombardi, Z.G. Ivanov, T. Claeson, and U. Scotti di Uccio, IEEE Trans. Appl. Supercond. **9**, 3652 (1999).
- ⁸L.G. Aslamazov and S.V. Lempitskii, Zh. Éksp. Teor. Fiz. **82**, 1671 (1982) [Sov. Phys. JETP **55**, 967 (1982)]; S.V. Lempitskii, *ibid.* **85**, 1072 (1983) [**58**, 624 (1983)]; A.D. Zaikin, *ibid.* **84**, 1560 (1983) [**57**, 910 (1983)].
- ⁹V.S. Shumeiko, G. Wendin, and E.N. Bratus, Phys. Rev. B **48**, 13 129 (1993); L.Y. Gorelik, V.S. Shumeiko, R.I. Shekhter, G. Wendin, and M. Jonson, Phys. Rev. Lett. **75**, 1162 (1995).
- ¹⁰B.J. van Wees, K.M.H. Lenssen, and C.J.P.M. Harmans, Phys. Rev. B **44**, 470 (1991).
- ¹¹A.F. Volkov, Phys. Rev. Lett. **74**, 4730 (1995).
- ¹²A.F. Volkov and H. Takayanagi, Phys. Rev. B **56**, 11 184 (1997); F.K. Wilhelm, G. Schön, and A. Zaikin, Phys. Rev. Lett. **81**, 1682 (1998); S.K. Yip, Phys. Rev. B **58**, 5803 (1998).
- ¹³A.F. Andreev, Zh. Éksp. Teor. Fiz. **46**, 1823 (1964) [Sov. Phys. JETP **19**, 1228 (1964)].
- ¹⁴G. Wendin and V.S. Shumeiko, J. Phys. Chem. Solids **56**, 1773 (1995); Phys. Rev. B **53**, R6006 (1996).
- ¹⁵L.F. Chang and P.F. Bagwell, Phys. Rev. B **55**, 12 678 (1997); H.T. Ilhan, H.V. Demir, and P.F. Bagwell, *ibid.* **58**, 15 120 (1998); H.Tolga Ilhan and P.F. Bagwell, J. Appl. Phys. **84**, 6758 (1998).
- ¹⁶P. Samuelsson, V.S. Shumeiko, and G. Wendin, Phys. Rev. B **56**, R5763 (1997).
- ¹⁷L.G. Aslamazov, A.I. Larkin, and Y.N. Ovchinnikov, Zh. Éksp. Teor. Fiz. **55**, 323 (1968) [Sov. Phys. JETP **28**, 171 (1969)]; I.O. Kulik, *ibid.* **57**, 1745 (1969) [**30**, 944 (1970)]; A.V. Svidzinsky, T.N. Antsygina, and E.N. Bratus', *ibid.* **61**, 1612 (1971) [**34**, 860 (1972)].
- ¹⁸A.V. Svidzinsky, T.N. Antsygina, and E.N. Bratus', J. Low Temp. Phys. **10**, 131 (1973).
- ¹⁹Volkov and Pavlovskii, Pis'ma Zh. Éksp. Teor. Fiz. **64**, 624 (1996) [JETP Lett. **64**, 670 (1996)].
- ²⁰M. Büttiker, Y. Imry, and M.Y. Azbel, Phys. Rev. A **30**, 1982 (1984).
- ²¹H. Nakano and H. Takayanagi, Solid State Commun. **80**, 997 (1991); Phys. Rev. B **47**, 7986 (1993).
- ²²A. Kadigrobov, A. Zagoskin, R.I. Shekter, and M. Jonson, Phys. Rev. B **52**, R8662 (1995).
- ²³F.W.J. Hekking and Yu. V. Nazarov, Phys. Rev. Lett. **71**, 1625 (1993); Phys. Rev. B **49**, 6847 (1994).
- ²⁴P.G. de Gennes, *Superconductivity in Metals and Alloys* (Addison-Wesley Publishing, Reading, MA, 1989).
- ²⁵K.K. Likharev, Rev. Mod. Phys. **51**, 101 (1979).
- ²⁶R. Landauer, IBM J. Res. Dev. **1**, 223 (1957); M. Büttiker, Phys. Rev. Lett. **57**, 1761 (1986).
- ²⁷P.F. Bagwell, Phys. Rev. B **46**, 12 573 (1992).
- ²⁸V.S. Shumeiko, E.N. Bratus', and G. Wendin, Fiz. Nizk. Temp. **23**, 249 (1997) [Low Temp. Phys. **23**, 181 (1997)].
- ²⁹W. Haberkorn, H. Knauer, and J. Richter, Phys. Status Solidi B **47**, K161 (1978); A. Furusaki and M. Tsukada, Physica B **165-166**, 967 (1990).
- ³⁰U. Gunsenheimer, U. Schüssler, and R. Kümmel, Phys. Rev. B **49**, 6111 (1994).
- ³¹C. Ishii, Prog. Theor. Phys. **44**, 1525 (1970).
- ³²A.D. Zaikin and G.F. Zharkov, Zh. Éksp. Teor. Fiz. **78**, 721 (1980) [Sov. Phys. JETP **51**, 364 (1980)]; **81**, 1781 (1981) [**54**, 944 (1981)].
- ³³U. Schüssler and R. Kümmel, Phys. Rev. B **47**, 2754 (1993); A. Chrestin, T. Matsuyama, and U. Merkt, *ibid.* **49**, 498 (1994); G. Wendin, V.S. Shumeiko, P. Samuelsson, and H. Takayanagi, Jpn. J. Appl. Phys., Part 1 **38**, 354 (1999).
- ³⁴H.A. Blom, A. Kadigrobov, A.M. Zagoskin, R.I. Shekter, and M. Jonson, Phys. Rev. B **57**, 9995 (1998).
- ³⁵G. Wendin and V.S. Shumeiko, Superlattices Microstruct. **4**, 569 (1996).
- ³⁶C.W.J. Beenakker and H. van Houten, *Single Electron Tunneling and Mesoscopic Devices* (Springer, Berlin, 1991).
- ³⁷V.T. Petrashov, V.N. Antonov, P. Delsing, and T. Claeson, Pis'ma Zh. Éksp. Teor. Fiz. **60**, 589 (1994) [JETP Lett. **60**, 606 (1994)]; B.J. van Wees, S.G. den Hartog, and A.F. Morpurgo, Phys. Rev. Lett. **76**, 1402 (1996); V.T. Petrashov, R.S. Shaikhaidarov, and I.A. Sosnin, Pis'ma Zh. Éksp. Teor. Fiz. **64**, 789 (1996) [JETP Lett. **64**, 839 (1996)]; S.G. den Hartog, C.M.A. Kapteyn, B.J. van Wees, T.M. Klapwijk, W. van der Graaf, and G. Borghs, Phys. Rev. Lett. **76**, 4592 (1996).
- ³⁸For a review of this subject, see C.J. Lambert and R. Raimondi, J. Phys.: Condens. Matter **10**, 901 (1998), and references therein.
- ³⁹B.Z. Spivak and D.E. Khmel'nitskii, Pis'ma Zh. Éksp. Teor. Fiz. **35**, 334 (1982) [JETP Lett. **35**, 412 (1982)].
- ⁴⁰B.L. Altshuler, D.E. Khmel'nitskii, and B.Z. Spivak, Solid State Commun. **48**, 841 (1983).
- ⁴¹M. Leadbeater and C.J. Lambert, Phys. Rev. B **56**, 826 (1997).
- ⁴²A.F. Volkov and A.V. Zaitsev, Phys. Rev. B **53**, 9267 (1996).
- ⁴³A. Dimoulas, J.P. Heida, B.J. van Wees, T.M. Klapwijk, W. van der Graaf, and G. Borghs, Phys. Rev. Lett. **74**, 602 (1995).
- ⁴⁴S.G. den Hartog, C.M.A. Kapteyn, B.J. van Wees, T.M. Klapwijk, W. van der Graaf, and G. Borghs, Phys. Rev. Lett. **77**, 4954 (1996); V.T. Petrashov, R.Sh. Shaikhaidarov, I.A. Sosnin, P. Delsing, T. Claeson, and A. Volkov, Phys. Rev. B **58**, 15 088 (1996).
- ⁴⁵A.F. Morpurgo, B.J. van Wees, T.M. Klapwijk, and G. Borghs, Phys. Rev. Lett. **79**, 4010 (1997).
- ⁴⁶V.N. Antonov, H. Takayanagi, F.K. Wilhelm, and A.D. Zaikin, Europhys. Lett. **50**, 250 (2000).
- ⁴⁷V.C. Hui and C.J. Lambert, Europhys. Lett. **23**, 203 (1993); C.J. Lambert and S.J. Robinson, Physica B **194-196**, 1641 (1994).
- ⁴⁸V.T. Petrashov, V.N. Antonov, P. Delsing, and T. Claeson, Phys. Rev. Lett. **70**, 347 (1993).
- ⁴⁹K. Neurohr, Th. Schäpers, J. Malindretos, S. Lachenmann, A.I. Braginski, H. Lüth, M. Behet, G. Borghs, and A.A. Golubov, Phys. Rev. B **59**, 11 197 (1999).
- ⁵⁰U. Fano, Phys. Rev. **124**, 1866 (1961).
- ⁵¹This formula was obtained in Ref. 32.